Supplementary Information for

Megaphylogeny resolves global patterns of mushroom evolution

Torda Varga, Krisztina Krizsán, Csenge Földi, Bálint Dima, Marisol Sánchez-García, Santiago Sánchez-Ramírez, Gergely J. Szöllősi, János G. Szarkándi, Viktor Papp, László Albert, William Andreopoulos, Claudio Angelini, Vladimír Antonín, Kerrie W. Barry, Neale L. Bougher, Peter Buchanan, Bart Buyck, Viktória Bense, Pam Catcheside, Mansi Chovatia, Jerry Cooper, Wolfgang Dämon, Dennis Desjardin, Péter Finy, József Geml, Sajeet Haridas, Karen Hughes, Alfredo F. Justo, Dariusz Karasiński, Ivona Kautmanova, Brigitta Kiss, Sándor Kocsubé, Heikki Kotiranta, Kurt M. LaButti, Bernardo E. Lechner, Kare Liimatainen, Anna Lipzen, Zoltán Lukács, Sirma Mihaltcheva, Louis Morgado, Tuula Niskanen, Machiel E. Noordeloos, Robin A. Ohm, Beatriz Ortiz-Santana, Clark Ovrebo, Nikolett Rácz, Robert Riley, Anton Savchenko, Anton Shiryaev, Karl Soop, Viacheslav Spirin, Csilla Szebenyi, Michal Tomšovský, Rodham E. Tulloss, Jessie Uehling, Igor V. Grigoriev, Csaba Vágvölgyi, Tamás Papp, Francis M. Martin, Otto Miettinen, David S. Hibbett, László G. Nagy

Published in Nature Ecology and Evolution.

This PDF file includes:

Supplementary Notes 1 to 8

Supplementary Figures 1 to 10

Supplementary Tables 1 to 8

Captions for Supplementary Data 1 to 7

Table of contents

Supplementary Note 1.: Phylogenomic analysis

Phylogenomics results - The phylogenomic analysis of Agaricomycotina included 104 genomes from 18 orders of the Agaricomycetes, as well as Dacrymycetes and Tremellomycetes (Supplementary Table 1.). We detected 663 gene families that contained a single gene per species or, if multiple genes per species were found they were inparalogs of each other. Of these, 650 contained genes from at least 75% of the species, which were concatenated into a supermatrix of 141.951 amino acid sites. Our analyses are in agreement with previous phylogenomic studies, but included members of Phallales, Gomphales and Thelephorales in phylogenomic studies for the first time.

Sensitivity analysis - Rapidly evolving sites can be a source of noise and may lead to incorrect topologies due to model violations; removal of these sites can improve phylogenetic signal[1]. To test the robustness of our results, ambiguously aligned amino acid sites were removed in an incremental manner. We discarded 8.5–55.2% of the sites of the original dataset in six steps, resulting in incrementally shorter and more conserved datasets, which, however, conferred minor changes in the inferred topologies and bootstrap values, which were limited to weakly supported branches. For example, the Pluteaceae proved to have an unstable position: in the original dataset it was placed as a weekly supported (BS 67%) sister group of Amanitaceae whereas it clustered together with the Tricholomatineae (sensu Dentinger et al.[2]) upon removal of 36.8% of the original dataset (BS 32%). Removal of 50.1% of the sites yielded a tree topology on which the Pluteaceae grouped together with the Macrocystidiaceae (BS 45%) (Supplementary Fig 2. C-F). Other changes observed upon the exclusion of 8.5–24.3 % of the original dataset were the repositioning of *Fibroporia radiculosa* as the earliest branching taxon of the antrodia clade. However, upon further exclusion of sites, this taxon returns to its original position as, the sister group of *Postia placenta* (BS 100%) on an unsupported branch (BS <50%) in the antrodia clade of Polyporales (Supplementary Fig 2. A, B). The exclusion of 24.3–36.8 % of the original dataset caused the reordering of groups in the Phallales-Geastrales-Gomphales-Trechisporales. It has also led to the relocation of *Sistotremastrum niveocremeum* (Supplementary Fig 2. B, C).

Phylogenomic relationships in the Agaricomycotina - Our trees confirmed previous results for most branches, although we inferred stronger support for certain groupings or contradicting relationships compared to previous genome-based or multigene studies. In the next section, we discuss nodes of the Agaricomycotina in detail that deviate from previous studies in placement. The Tremellomycetes, represented by two members of Tremellales (*Tremella mesenterica* and *Cryptococcus neoformans* var. *grubii*), were used as an outgroup. The Dacrymycetes formed a strongly supported sister group of Agaricomycetes in contrast with Zhao et al.[3], where this topology was not well-supported (BS 55%), but in agreement with the majority of other phylogenomic studies[4–6]. Our phylogeny supports the early divergence of the Cantharellales, Sebacinales and Auriculariales in the Agaricomycetes as it has been described previously[4–7]. The Phallomycetidae in our analysis showed sister group relationship with the Trechisporales (BS 85%, Supplementary Fig 1) in accordance previous studies[3], although some studies suggested that the Trechisporales forms an independent lineage branching prior to Hymenochaetales and the remaining Agaricomycetes[5,8,9]. The position of the clade formed by Gloeophyllales, Jaapiales, and Corticiales remained ambiguous previously[8]. Some studies suggested this clade to be a sister of the Polyporales[3,5] or of the Agaricomycetidae[10], while others suggested that this clade is the sister group to the clade formed by the Russulales and Agaricomycetidae[6,8,11]. Additionally, Binder et al.[12] inferred a clade comprising *Gloeophyllum*, corticioid, russuloid and polyporoid clades, but not the Jaapiales. This latter was placed as the

sister group of the euagarics, boletoid and athelioid clades. Our results showed partial congruence with these findings: the Gloeophyllales, Jaapiales and Corticiales formed a strongly supported clade sister to (BS 93%) the clade formed by Russulales, Theleophorales, and Polyporales. On a higher-level, these groups were sister to the Agaricomycetidae. In line with this, our phylogeny did not confirm the sister group relationship of Russulales and Agaricomycetidae[3,6–9]. We inferred the Russulales as the sister to the clade formed by the Polyporales, Gloeophyllales, Jaapiales and Corticiales (BS 93%). Within this clade the Russulales was the sister group of the Thelephorales and Polyporales (BS 56%) (Supplementary Fig. 1). The sister group relationship of the Polyporales and Thelephorales was mentioned by Hibbett[4] and Matheny[9] and was confirmed in these study with strong support (BS 100%). However, the Thelephorales was represented by only a single species (*Thelephora ganbajun*), as more sequenced genomes will be available, this relationship should be further tested.

The monophyly of Polyporales has been robustly demonstrated by several previous studies[7,11–13]; however, the composition and support of the subclades therein remained unresolved. Similarly to the 356- and 71-gene-based phylogeny of Binder et al.[11] the four major clades of the Polyporales (antrodia clade, gelatoporia clade, core polyporoid clade, phlebioid clade) and their branching order were confirmed with strong support (BS 100%) using an extended sampling of genomes in this study. Whereas our taxon set improved sampling in the gelatoporia, the antrodia, the core polyporoid and the phlebioid clades compared to Binder et al.[11], no new genomes were involved in the phylogenomic analysis from the more problematic "residual polyporoid" clade.

Our results did not resolve the two higher-level clades suggested by Justo et al.[13] based on nrITS, nrLSU and *rpb1*: one contained *Candelabrochaete africana*, the "phlebioid" and "residual polyporoid" clades, while the other included the "core polyporoid", "gelatoporia", "antrodia" and "skeletocutis-tyromyces" groups. Our dataset did not include species from the "residual polyporoid" and "*Tyromyces*" clades, however. Although the antrodia clade itself was well supported, within the clade we found poor support for the branching at *Fibroporia radiculosa* and *Postia placenta*, and for the grouping of this clade with that formed by *Wolfiporia cocos* and *Laetiporus sulphureus* var. *sulphureus*. For clarifying the branching order and relationship of these clades the inclusion of additional genomes will be necessary.

The topology of the major groups of Agaricomycetidae is in accordance with previous phylogenomic[5,6,8] and phylogenetic studies[9,10,14–17] that supported the sister group relationship of Amylocorticiales-Atheliales and Boletales, which together formed the sister group of the Agaricales. Within the Boletales, branches are well supported and are in full agreement with the results based on the phylogenetic relationships inferred from 5.8S rRNA, *rpb1*, *rpb2*, and *tef1* in the study of Binder et al.[10] and previous phylogenomic inferences[3,5,6].

Relationships in the Agaricales were largely congruent with that of Dentinger et al.[2]. Within the Agaricales we determined a highly supported (BS 100%) clade formed by *Schizophyllum commune* and *Fistulina hepatica* that corresponds to the Schizophyllineae[2], but this is in contrast with the recent study of Zhao et al.[3], which found the Shcizophyllaceae and Pterulaceae to group together, based on a six-gene phylogeny. On our tree, the Schizophyllaceae branched after the Hygrophorinae (consisting of the Clavariaceae and Hygrophoraceae) and Pleurotinae (including the Pleurotaceae and Pterulaceae) split off of the backbone, which is consistent with the tree of Dentinger et al.[2], but is in contrast with other previous studies[5,6] with sparser taxon sampling. Additionally, we resolved the weakly supported clade of Physalacriaceae, Cyphellaceae, and hydropoid clade, among which the Cyphellaceae and hydropoid clade are sister groups and branch before the Physalacriaceae (BS 97%). Furthermore, the Marasmiineae clade according to

Dentinger et. al.[2] was supplemented by *Dendrothele bisporus* in our dataset, which formed the strongly supported sister lineage (BS 100%) of Omphalotaceae.
The clade corresponding to Pluteineae[2] forms a sister group of the clade equivalent to Agaricineae[2] in our results (BS 63%), but this relationship received lower support than that found by Dentinger et al. (BS 80%). Besides, we found the same moderately supported sister relationship between the Amanitaceae and Pluteaceae (BS 67%) as Dentinger et al. (BS 69%), even though, the Pluteaceae was supplemented with *Pluteus cervinus* in our study. The Pluteaceae proved unstable in our sensitivity analysis as well: with the removal of increasing amounts of the fastest-evolving sites from original dataset the Pluteaceae either grouped together with the Tricholomataceae (BS 32%) or was paraphyletic (BS 61%), but no longer formed a monophyletic group together with the Amanitaceae. Future studies should include either more species of Pluteaceae or construct more informative datasets to help resolve this contentious part of the Agaricales phylogeny.
A well-supported clade corresponding to the Tricholomatineae (BS 100%)[2] could be resolved in our study. A strongly supported sister relationship of *Macrocystidia cucumis* and *Infundibulicybe gibba* (BS 100%) was inferred for first time here, which resolved the inconsistent placement of these taxa in the study of Dentinger et al.[2].
Recent phylogenomic[2,5,6] and phylogenetic[3] studies found the Psathyrellaceae to branch off before the Hydnangiaceae, except Matheny et al.[14], who proposed the sister group relationship of these two groups. Our results, involving additional two species of the Psathyrellaceae (*Coprinopsis marcescibilis*, *C. micaceus*), but only one species of Hydnangiaceae (*Laccaria bicolor*) confirm Matheny et al's results and supports the sister group relationship of Hydnangiaceae and Psathyrellaceae (BS 100%).

Supplementary Note 2.: Phylogenetic analyses of the 5,284 species dataset

Sequence alignment - Overall 5,284 species have been sampled from the Agaricomycetes, Dacrymycetes and Tremellomycetes from which the latter was used as an outgroup. Three loci, nrLSU (4,835 species) *rpb2* (1,252 species) and *ef1-α* (721 species) were included in the analyses. The final alignment contained 6,905 characters in total, from which we excluded 1,168 ambiguously aligned sites (including intronic regions) to obtain a final length of 5,737 characters. Of this, the length of individual partitions was 1,052 for *tef1-α*, 2,768 for nrLSU and 1,917 for *rpb2*.

Phylogenetic tree reconstruction: Maximum Likelihood analyses - Maximum likelihood (ML) trees for the 5,284-species dataset were inferred as it was described in the Materials and Methods. We performed 245 ML inferences and tested whether these trees adequately represented the plausible set of topologies given the alignment by examining the Robinson-Foulds (RF) distances across trees. Because the maximum, the average and the minimum of the RF values were saturated (Supplementary Fig. 3.) we stopped to generate trees after the 247th ML run.

Supplementary Note 3.: Newly sequenced genomes

To fill some gaps in the genome-scale phylogeny of the Agaricomycetes, we sequenced the genomes of nine species, listed in Supplementary Table 1. Sequencing was performed on either Illumina or PacBio platforms and resulted in 74x - 141x coverage and assembly sizes ranging from 32 Mb to 131 Mb. The largest assembly was obtained for *Dendrothele bispora*, a highly reduced corticioid species in the Agaricales. This species also had the highest number of predicted genes (33,645). In terms of fragmentation, *Heliocybe sulcata* had the least fragmented genome with 87 scaffolds, followed by *Pterula gracilis* and *Crucibulum laeve*. Uniformly, 40 - 62% of the predicted genes had InterPro-based annotations.

The rationale for selecting species was based on current sampling of Agaricomycetes orders and families within the Agaricales. Of the nine species, *Crucibulum laeve* is the first sequenced representative of the Nidulariaceae, an enigmatic family in the Agaricales containing 'bird's-nest fungi' with highly specialized morphologies and dispersal strategies. Similarly, *Pluteus cervinus* is a representative of the Pluteaceae, from which only *Volvariella volvacea* has been available previously. The *Pluteus* genome was sequenced from field-collected fruiting bodies and surprisingly contained <1% of bacterial contaminating sequence reads. *Pterula gracilis* is an early-diverging member of the Agaricales and the first sequenced species in the Pterulaceae. It shows affinities to pleurotoid and schizophylloid species and fills an important gap in the genomic sampling of the Agaricales. Outside the Agaricales, we sequenced *Peniophora* sp, which is an early-branching member of the Russulales (Peniophoraceae), whereas *Polyporus arcularius* and *Heliocybe sulcata* belong to the Polyporales and Gloeophyllales, respectively.

<u>*Assembly and annotation*</u> - Genomic reads from both libraries were QC filtered for artifact/process contamination and assembled together with AllPathsLG v. R49403[18]. Illumina reads of stranded RNA-seq data were used as input for de novo assembly of RNA contigs, assembled into consensus sequences using Rnnotator (v. 3.4)[19]. All genomes were annotated using the JGI Annotation Pipeline and made available via the JGI fungal portal MycoCosm[20]. Genome assemblies and annotation were also deposited at DDBJ/EMBL/GenBank (see main text for accession numbers).

Supplementary Note 4.: Molecular dating

Assessing fossil calibration signal - Both PhyloBayes and FastDate analyses reached convergence (data not shown). The fossil cross-validation analysis suggested that there is no conflict between fossil calibrations points (Supplementary Fig. 4.), so we used all fossils in subsequent analyses. By comparing the age estimates for clades with that from recent molecular clock studies[6,7] we found that our estimates were comparably older. For example the emergence of Agaricales was dated to 90 and 108 mya by Floudas et al.[7] and Kohler et al.[6], respectively while our mean estimated ages ranged between 160-182 mya depending on the tree analyzed (Supplementary Data 2). The differences could come from the different data set (the analyses of Floudas et al.[7] and Kohler et al.[6] based on genomes), taxon sampling density or the calibration schemes used in the analyses. To address the causes of the difference in age estimates, we performed molecular dating on genomic data under various calibration schemes.
The following fossils were considered as potential calibration points, but were excluded either because of uncertainties in their taxonomic placement or redundancy with other, more informative fossils for our dataset:

Fomes mattirolii - Age: Miocene (5.3–23 million years ago) Site: Libya. Taxonomic assignment uncertain and the fossil is too recent (Miocene) to inform calibration of the tree. Reference: Zuffardi-Comerci, R., 1934. Fomes (Polyporus) Mattirolii n. sp. nel Miocene della Libia. Missione Scientifica della Reale Accademia d'Italia a Cufra (1931-IX), vol. 3, pp. 58–60.

Archeterobasidium syrtae - Age: Miocene (5.3–23 million years ago) Site: Libya. Similar to *Ganodermites libycus*, belongs to Ganodermataceae, but too recent (Miocene) to be informative. Reference: Koeniguer, J.C., Locquin, M.V., 1979. Un polypore fossile à spores porées du Miocène de Libye: Archeterobasidium syrtae, gen. et sp. nov. In: Ministère des Universités Comité des Travaux Historiques et Scientifiques (Ed.), Comptes Rendus du 104e Congrès National des Sociétés Savantes, Bordeaux, 1979, fasc. I (Paléobotanique). Paris (France), Bibliothèque Nationale, pp. 323–329.

Fomites libyae - Age: Miocene (5.3-23 million years ago) Site: Libya. No photo available of the fossil, presumably similar to *Fomes*. Too recent (Miocene). Reference: Locquin, M.V., Koeniguer, J.C., 1981. Un nouveau polypore fossile du Miocène de Libye: Fomites libyae Locquin et Koeniger, gen. et sp. nov. In: Ministère des Universités comité des Travaux Historiques et Scientifiques (Ed.), Comptes Rendus du 106e Congrès National des Sociétés Savantes, Perpignan, 1981, fasc. I (Paléontologie). Paris (France), Bibliothèque Nationale, pp. 107–117.

***Polyporus* sp.** - Age: Miocene (5.3–23 million years ago) Site: Libya. No photo of the fossil found, publication could not be accessed. Reference: Mayr, H., 2006. Fossilien. BLV Buchverlag GmbH, Munich (Germany), 255 pp.

Ganoderma adspersum - Age: Miocene (5–23 million years ago) Site: Netherlands. Too recent. Reference: Fraaye, R.H.B., Fraaye, M.W., 1995. Miocene bracket fungi (Basidiomycetes, Aphyllophorales) from the Netherlands. Contrib. Tert. Quat. Geol. 32, 27–33.

Ganoderma applanatum - Age: Pleistocene (2.6–0.01 million years ago) Site: Alaska, USA. Too recent. Reference: Chaney, R.W., Mason, H.L., 1936. A Pleistocene flora from Fairbanks, Alaska. Amer. Mus. Nat. Hist. Novitates 877, 1–17.

Ganoderma lucidum - I.Age: Pleistocene (2.6–0.01 million years ago) Site: Alaska, USA. II.Age: Pleistocene (2.6–0.01 million years ago) and Holocene (0.01 ma–today). Too recent. References: Chaney, R.W., Mason, H.L., 1936. A Pleistocene flora from Fairbanks, Alaska. Amer. Mus. Nat. Hist. Novitates 877, 1–17. Kopczyński, K., 2006. Zapis kopalny grzybów i organizmów grzybopodobnych (Fossil record of fungi and pseudofungi). Prz. Geol. 54, 231–237 (in Polish with an English abstract).

Fomes idahoensis - Age: Pliocene (5.3–2.6 million years ago) Site: Idaho, USA, Too recent. Reference: Brown, R. W., (1940): A bracket fungus from the late Tertiary of southwestern Idaho. – Ibidem, 30: 422–424., Buchwald, N. F., (1970): Fomes idahoensis Brown. A fossil polypore fungus from the Late Tertiary of Idaho,U. S. A. – Friesia 9: 339–340.

Trametites ginkgoides - Age: Pliocene (5.3–2.6 million years ago) Site: Germany, Too recent. References: Straus, A., 1952a. Beiträge zur Pliozänflora von Willershausen III. Die niederen Pflanzengruppen bis zu den Gymnospermen. Palaeontogr., Abt. B 93, 1–44., Straus, A., 1952b. Pilze aus dem Pliozän von Willershausen (Kr. Osterode, Harz). Z. Pilzkd. 21, 11–14.

Appianoporites vancouverensis - Age: Eocene (56–34 million years ago) Site: Vancouver, Canada. Redundant with Quatsinoporites. Reference: Selena, Y. S., Randolph, S. C., Ruth, A. S., Cretaceous and Eocene poroid hymenophores from Vancouver Island, British Columbia Mycologia, 96(1), 2004, pp. 180–186.

Coprinites dominicanus - Age: Miocene (20–16 million years ago) Site: Dominican Republic, Taxonomic assignment uncertain, too recent to calibrate higher-level categories (e.g. Agaricales). Reference: George, O. P., Jr. and Rolf, S., Upper Eocene Gilled Mushroom from the Dominican Republic Science, New Series, Vol. 248, No. 4959 (Jun. 1, 1990), pp. 1099–1101.

Protomycena electra - Age: Miocene (25–15 million years ago) Site: Dominican Republic. Redundant with *Archaeomarasmius*, but more recent. Reference: Hibbett, D.S., Grimaldi, D.S., Donoghue, M.J., (1997). Fossil mushrooms from Miocene and Cretaceous Ambers and the evolution of Homobasidiomycetes American Journal of Botany 84 (8), 981–991.

Aureofungus yaniguaensis - Age: Miocene (25–15 million years ago) Site: Dominican Republic. Too recent, taxonomic position uncertain. Reference: Hibbett D., Binder M., Zheng, W., Yale, G., Another fossil agaric from Dominican amber Mycologia, 95(4), 2003, pp. 685–687.

Cyathus dominicanus - Age: Oligocene–Miocene (30–15 million years ago) Site: Dominican Republic. Redundant with *Nidula baltica* but more recent. Reference: Poinar, Jr. G., (2014). Bird's nest fungi (Nidulariales: Nidulariaceae) in Baltic and Dominican amber. Fungal Biology, 118(3), 325–329.

Bovista plumbea - Age: Pleistocene (2.6–0.01 million years ago) Site: Alaska, USA. Too recent. Reference: Chaney, R.W., Mason, H.L., 1936. A Pleistocene flora from Fairbanks, Alaska. Amer. Mus. Nat. Hist. Novitates 877, 1–17.

Lycoperdites tertiarius - Age: Oligocene–Miocene (26–22 million years ago) Site: Mexico Position as a true puffball (Lycoperdaceae) is uncertain. Reference: POINAR, G.O., JR.,

2001. Fossil Puffballs (Gasteromycetes: Lycoperdales) in Mexican amber. Historical Biol. 15,219–222.

Geastrum tepexensis - Age: Miocene–Pleistocene (8–5 million years ago) Site: Mexico. Taxonomically it could either belong to Geastrales or *Astraeus*. Reference: Magallon-Pueble, S. & R.S. Cervallos-Ferriz, 1993. A fossil earthstar (Geasteraceae; Gasteromycetes) from the Late Cenozoic of Pueblo, Mexico. Amer. J. Bot. 80, 1162–1167.

Geastroidea lobata - Age: Late Cretaceous (72-66 million years ago) Site: Mongolia. The characters of the fossil cannot be evaluated based on the photographs. Reference: Krassilov, V.A., Makulbekov, N.M., 2003. First find of Gasteromycetes (fungi) in the Cretaceous deposits of Mongolia. Paleontological Journal 37, 439–442.

Palaeogaster micromorphus - Age: Mid-Cretaceous (97–110 million years ago) Site: Myanmar (Burma). Taxonomic assignment uncertain. Reference: George, O. P., Jr., Dônis da Silva, A., Iuri, G. B., A Gasteroid fungus, Paleogaster micromorpha gen. & sp. nov. (Boletales) in Cretaceous Myanmar Amber. Journal of the Botanical Research Institute of Texas 8(1)), 139–143. 2014.

Palaeoclavaria burmitis - Age: Mid-Cretaceous (110–100 million years ago) Site: Myanmar (Burma) Taxonomic affinity as a clavarioid fungus is doubtful. Reference: Poinar, G.O., JR. & A.E. Brown., 2003. A non-gilled hymenomycete in Cretaceous amber. Mycological Res. 107: 763–768.

Molecular clock analysis of genome-scale data - The reduced dataset used for molecular clock dating contained 105 species, 70 genes and 18,917 amino acid characters. Cross-validation analyses in r8s yielded 10 or 100 as the best smoothing parameter for penalized likelihood analyses. In mcmctree, all MCMC chains converged to stationary distributions as judged from log-likelihood values and the three independent MCMC replicates yielded congruent age estimates. We found that models with a scale parameter of 1000 for the gamma-Dirichlet prior were >127 times more unlikely than models with a scale parameter 100 or 10, so we chose a scale parameter of 100 for subsequent analyses in mcmctree.

We first assessed the impact of the placement of calibration points on the tree. When we placed the fossils used by Kohler et al.[6] to the exact same positions on the tree as in the previous study, we obtained similar, but slightly older estimates for most nodes: 126 myr and 131 myr for the Agaricales and the Agaricomycetidae, compared to 108 myr and 125 myr by Kohler et al.[6], respectively ("Kohler et al. calibration scheme 1") (Supplementary Data 2). Assigning suilloid ectomycorrhizae and *Archaemarasmius* to the more precisely defined ancestors of the Suillaceae and of the marasmioid clade (due to new genome sequences available to us) yielded considerably older estimates, 169 myr and 176 myr for the Agaricales and the Agaricomycetidae, respectively ("Kohler et al. calibration scheme 2"). Adding another 6 fossils to the analysis ("Default calibration scheme") yielded 156 myr and 162 myr for these nodes, a comparably small change from the 2-fossil calibration scheme, suggesting that molecular age estimates are primarily driven by the precision of the placement of fossil calibrations on the tree and to a smaller extent by the set of fossil calibration points used (Supplementary Data 2).

The divergence times estimated by mcmctree were generally older than those estimated by r8s and were more similar to the ages inferred with the 5,284-species tree (Supplementary Fig. 5). The mean age of the Agaricomycetidae was estimated at 182 myr, 20 myr older than by r8s, but 3 myr younger than the mean across the 10 chronograms containing 5,284 species. The age of

the Agaricales and the Boletales were inferred at 175 and 166 myr, as opposed to 156 and 150 by r8s, respectively. Larger differences were obtained for more ancient nodes, which might be related to differences in how the root was constrained in the different analyses. The mrca of Agaricomycetes was inferred at 317 myr, 46 myr older than the date given by r8s. That of the Agaricomycetes and Dacrymycetes was inferred at 385 myr in mcmctree as opposed to 314 myr in r8s. Despite these differences, analyses in mcmctree and r8s are consistent in that they both suggest that the Agaricomycetidae and most orders therein originated in the Jurassic period.

Supplementary Note 5.: Trait evolution

Analyses of character evolution - Analyses of the evolution of agaricoid fruiting body type in BayesTraits showed that gains of the pileate-stipitate morphology were favored during evolution (Supplementary Data 7, Fig. 3/d). The average transition rates from the non-pileate towards the pileate-stipitate state (q_{01}) were 6.9–51.5 times higher than in the reverse direction (q_{10}) depending on the method (ML or MCMC). Constraining the rates of gain and loss to be equal ($q_{01} = q_{10}$) resulted in significantly lower likelihoods (40 log-likelihood units, logBF: 47), suggesting that models with equal gain and loss rates can be rejected. The biggest differences from the null model were found when the rate of gain of the pileate-stipitate morphology (q_{01}) was forced to be zero (383 log-likelihood units, log BF: 382). Models with the reverse rate (q_{10}, loss of pileate-stipitate type) constrained to zero were also significantly different from the null model (159 log-likelihood units, log BF: 157), which suggests that the transition from pileate-stipitate to non-pileate types was also important during the evolution of mushroom forming fungi. Analyses performed under the BiSSE model yielded similar results (Supplementary Data 7, Fig. 3/d). In BISSE, the average transition rates from the non-pileate towards the pileate-stipitate state (q_{01}) were 13.2–14.2 times higher than in the reverse direction (q_{10}). All the constrained BiSSE models ($q_{01} = q_{10}$ or $q_{01} = 0$ or $q_{01} = 0$) yielded significantly worse likelihoods than the null model according to likelihood ratio tests ($p < 0.001$, Supplementary Data 7).

Ancestral character state reconstruction - We found that the transition rate matrices estimated during the ancestral state reconstruction (ASR) analyses contained highly similar values across trees in case of both traits (fruiting body types and substrate/host preference) examined in this study (Supplementary Data 3). In case of fruiting body types, species with resupinate or no fruiting bodies dominated the first periods of the evolution of Agaricomycetes. Then, around 180 million years ago, complex fruiting body types (agaricoid, cyphelloid, gasteroid/secotioid, coralloid/clavarioid) appeared and the cumulative posterior probability of the agaricoid type started to increase until it became the dominant fruiting body type (see Fig. 3 in main text). In parallel, the prevalence of resupinate fruiting body types decreased. This essentially suggests that resupinate fruiting bodies were phased out by the agaricoid type as the most widespread fruiting body morphology. It should be noted, however, that this does not necessarily mean that resupinate lineages became less diverse or went extinct, rather, it means that the proliferation of agaricoid lineages leads to resupinate ones sharing a lower fraction of the cumulative posterior probability.

ASR of species' preference for substrate (either gymnosperm or angiosperm) revealed that the Boletales, Polyporales, Russulales, Hymenochaetales and Phallomycetidae, all dated close to or in the Jurassic period, likely had ancestors with a gymnosperm preference (posterior probability, PP > 0.70). The MRCA of the Agaricales had an unresolved substrate preference (PP of gymnosperm substrate: 0.54). Of the orders dated to the Jurassic, only the MRCA of the Sebacinales and that of the Cantharellales showed higher probabilities for angiosperm than gymnosperm substrates (PP = 0.91 and 0.87, respectively). Smaller orders that emerged after the Jurassic were associated with either gymno- or angiosperms. The Trechisporales and the Corticiales were inferred to be ancestrally angiosperm-associated, while the most recent common ancestors of the Thelephorales, the Jaapiales, the Atheliales, the Gloeophyllales and the Amylocorticiales likely were associated with gymnosperms. The MRCA of the Lepidostromatales had no clear preference towards either plant groups (Supplementary Data 3). The MRCA of Agaricomycetidae was inferred to have been associated with gymnosperms (PP =

0.83), like three of the orders therein (Boletales, Amylocorticiales and Atheliales), suggesting that the evolution of these species started with a close association with gymnosperms.
By comparing the posterior probabilities of substrate preference at ancient nodes and that of extant species we found that some clades underwent remarkable changes (Supplementary Data 3). We found that the MRCA of the Polyporales, that of the Russulales and of the Boletales was likely to associated with gymnosperms (PP = 0.88, 0.98 and 0.98, respectively), yet the extant species mostly associate with angiosperms (probability of having angiosperm substrate: 0.76, 0.64 and 0.64, respectively) suggesting a major shift from gymno- to angiosperm substrates during the evolution of these clades. On the other hand, our results suggest that substrate preferences of the Corticiales, the Trechisporales and the Auriculariales have not or just slightly changed during their evolution. The posterior probability of having an angiosperm substrate was inferred as 0.84, 0.88, and 0.79 respectively at the MRCA of these clades, which is similar to the current distribution of states (0.93, 0.80 and 0.74 respectively). Interestingly, all of these orders evolved when angiosperms became the dominant component of the flora (Corticiales: 101 mya, Trechisporales: 86 mya, Auriculariales: 134 mya), therefore their angiosperm substrate preference comes as no surprise.
These results have two interesting implications. First, the ASR analyses suggest that MRCA-s of orders that originated in gymnosperm and angiosperm dominated evolutionary periods had most likely been associated with gymnosperms (Boletales, Polyporales, Russulales, Hymenochaetales and Phallomycetidae) and angiosperms (Auriculariales, Corticiales, Trechisporales) ancestrally. Second, our inferences imply that ancestrally gymnosperm-associated orders (Polyporales, Russulales and Boletales) have undergone several substrate switches during their evolution, resulting in a dominance of angiosperm association among extant members. These switches might be correlated with transitions in the global availability of gymno- vs angiosperms as substrates or hosts for fungi during the late Cretaceous period[21]. Thus, it appears that the rise of the angiosperms during the Cretaceous period left a footprint on the substrate preference of mushroom-forming fungi, an intriguing case of co-evolution driven by trophic interactions between large clades of organisms.
By analysing the overall ASR patterns through time (Figure 3/b in the main text) we found that early Agaricomycetes nodes had equally distributed probabilities between gymnosperms and angiosperms as their ancestral substrate plant group. The summed posterior probability of having had a gymnosperm substrate started to increase around 275 million years ago and reached >0.95 across all ancestors around 200 mya. This pattern coincides with the dominance of conifers in the Triassic and Jurassic period. Around 170 mya an increase in the probability of having had an angiosperm substrate was inferred. After this period, we observed a steady increase in the share of posterior probability of angiosperm substrates, with extant substrate preference distribution dominated by them too (0.32 / 0.68 = gymnosperms / angiosperms).
It should be noted, that the interpretation of inferred ancestral states of host/substrate preference has limitations for nodes older than the Permian, which predate the origin or global expansion of gymno- and angiosperms[22,23]. We found evenly distributed posterior probabilities for gymno- and angiosperms for all pre-Permian nodes, which is biologically questionable given that these weren't ubiquitously present in these periods. However, such a result is necessarily inferred in ASR analyses, because of the lack of species in our datasets that would be associated with descendants of typical Carboniferous plants (e.g. pteridophytes). Because of this methodological limitation, we had drawn conclusions from only those clades which evolved after the inferred origin of gymno- and angiosperms.

Trait dependent diversification rate analyses - The trait dependent diversification rate analyses under the BiSSE model suggest that pileate-stipitate species have higher diversification rates than non-pileate species (Supplementary Data 7, Fig. 3/e). The speciation rate for the pileate-stipitate state was 1.35–1.42 times higher than that of the non-pileate state. Model tests revealed that the unconstrained models fit the data significantly better ($p < 0.001$, LRT) than models where the two state specific rates were constrained to be equal. The extinction rate of pileate-stipitate species was 1.19–8.57 times lower than that of non-pileate species, however, in this case the unconstrained model did not fit the data significantly better than a model where the state-specific extinction rates were constrained to be equal ($\mu_0 = \mu_1$, $p > 0.05$, LRT). These results suggest that pileate-stipitate species have significantly higher speciation rates, but not significantly different extinction rates than non-pileate ones.

Supplementary Note 6.: Analyses of mass extinction events

First, we calculated Bayes factors between CoMET models with and without a mass extinction event. This analysis showed that models with a mass extinction event were preferred over models without mass extinction events (mean Bayes factor: 25.7, Supplementary Table 3.). This suggests that our data supports the presence of at least one mass extinction event during the evolution of mushroom forming fungi. To infer the number of mass extinction events and their timing, we performed rjMCMC under CoMET models with varying numbers of mass extinction events and speciation and extinction rate changes. These analyses supported one or two mass extinction events depending on the tree analyzed (Supplementary Fig. 6). This result was robust to the choice of priors on the expected number of mass extinction events, expected rate changes and survival probability (data not shown). We found that every numerical parameter reached high effective sample size values (Supplementary Table 4; ESS>500), and showed convergence according to Geweke's statistics ($p > 0.05$), except the likelihood values which, in 7 out of 10 analyses didn't pass Geweke's test although they appear converged based on the likelihood diagnostic plots. The interval specific parameters converged in every time interval (Geweke's statistics: $p > 0.05$) and had high ESS values (>500).

The results suggest that a mass extinction event happened during the Jurassic period Supplementary Fig. 6), between 200 million years ago (mya) and 145 mya, with strong support ($\ln BF > 6$) in nine out of the 10 trees. A second, a strongly supported mass extinction event was also inferred, around 230 mya, in three out of the ten trees.

Supplementary Note 7.: Latitudinal diversity gradient hypothesis

The latitudinal diversity gradient (LDG) hypothesis posits that species richness increases from the poles towards the tropics. To test this, we analyzed both centroid latitudes as continuous traits and terrestrial ecoregions as discrete traits (see Methods) for each of the species for which sufficient geographic data could be obtained (4,429 species). We fitted multiple Quantitative State Speciation and Extinction (QuaSSE) models to the ten chronograms to find the model, which best describes the latitude dependent diversification rates of Agaricomycetes species. Based on log-likelihood values, we have found that the model with Gaussian speciation and constant extinction rate fits better to our data than any other examined model and that the latitude has no effect on the extinction rate (Supplementary Table 5). These findings were supported by likelihood ratio tests, which showed that only the Gaussian speciation and constant extinction models differed significantly from the null model (constant speciation and extinction rates). Therefore, we used this model to interpolate speciation rates into a 1 × 1 degree global map (Supplementary Fig. 7). We found that the speciation rate was highest between 20° and 40° in the temperate zone. This does not coincide with the zone of the highest sampling density (30°–60°) in our data. This result suggests that latitudinal diversification patterns are largely independent from sampling patterns in our data.

In discrete analyses of geographical diversification patterns we divided all terrestrial WWF ecoregions into either tropical or extra-tropical (Supplementary Fig. 8). We assigned one of three states to each species: tropical, extra-tropical or widespread (see Materials and Methods). Using these three states for each taxon, we fitted multiple constrained models and one full model of Geographic State Speciation and Extinction (GeoSSE[24]), in a maximum-likelihood framework. The constrained models consisted of: (b) speciation in the tropics is equal to speciation in the extra-tropical zone; (c) extinction in the tropics is equal to extinction in the extra-tropical zone; (d) dispersal to the tropics occurs at the same rate as dispersal to the extra-tropical zone. The unconstrained model had the highest log-likelihood value (Supplementary Table 6), which was significantly better that the log-likelihood of any of the constrained models, based on likelihood ratio tests. In MCMC analysis we found that species in extra-tropical regions have higher diversification rate than species in tropics. (Supplementary Data 5. Interestingly in the tropics the speciation rate was higher than in the extra-tropics but so was the extinction rate. Moreover the extinction rate was near to zero in the extra-tropics which resulted in higher net diversification rate for species in extra-tropical areas.

Supplementary Note 8.: Trait independent diversification rate analyses

Accounting for non-random and incomplete taxon sampling - Taxon sampling in any phylogenetic dataset is inevitably non-random in most cases (due to how well certain groups are researched) and incomplete for large taxonomic breadths, such as Agaricomycetes. To ensure that our dataset conforms to the randomness requirement of BiSSE and BAMM models, we adjusted our taxon sampling in the 5284-taxon phylogeny. We found that 390 genera (out of 782) were significantly over- (365) or undersampled (25) based on comparisons to genus-wise diversities obtained from Species Fungorum (see Materials and Methods). We reduced the number of over- and undersampled genera to 112 and 12, respectively (complete lists are given below), by randomly removing species from oversampled genera. The remaining oversampled genera mostly contained 1 or 2 species, meaning that we couldn't mitigate oversampling without removing the genus itself from the dataset (Supplementary Data 1). The sampling fractions of pileate-stipitate and non-pileate species were 0.147 and 0.160, respectively, which means a relatively even sampling across the different states. In concordance with this, we found congruent results between different sampling bias correction strategies (built-in sampling correction, using skeletal tree or no corrections) in preliminary BiSSE and BAMM analyses (data not shown). Although we detected no obvious effect of sampling bias corrections in the results, we applied the built-in corrections of the BiSSE and BAMM models in further analyses, because we wanted to fulfill all the theoretical assumptions of the models.

Genera that remained oversampled: *Acantholichen*, *Albatrellopsis*, *Aleurobotrys*, *Allopsalliota*, *Andebbia*, *Aphroditeola*, *Atractosporocybe*, *Australovuilleminia*, *Barcheria*, *Basidioradulum*, *Bertrandia*, *Biatoropsis*, *Bogbodia*, *Bondarcevomyces*, *Bothia*, *Botryohypochnus*, *Brunneocorticium*, *Bulbillomyces*, *Calocybella*, *Calvarula*, *Cantharellopsis*, *Caripia*, *Catatrama*, *Cibaomyces*, *Claustula*, *Coniolepiota*, *Crustodontia*, *Dendrocollybia*, *Dentipellopsis*, *Dictyopanus*, *Earliella*, *Eonema*, *Ertzia*, *Faerberia*, *Fevansia*, *Flavophlebia*, *Gastrocybe*, *Giacomia*, *Gigasperma*, *Globulicium*, *Globulisebacina*, *Gloeostereum*, *Granulobasidium*, *Guyanagaster*, *Gymnogaster*, *Gyrodontium*, *Haloaleurodiscus*, *Halocyphina*, *Hebelomina*, *Heinemannomyces*, *Heliocybe*, *Hemistropharia*, *Hydnomerulius*, *Hymenogloea*, *Kauffmania*, *Kjeldsenia*, *Laeticorticium*, *Laeticutis*, *Lampteromyces*, *Lepistella*, *Leucocortinarius*, *Limnoperdon*, *Mackintoshia*, *Mayamontana*, *Melanoporia*, *Membranomyces*, *Mycobonia*, *Mycopan*, *Myriostoma*, *Mythicomyces*, *Naiadolina*, *Neohygrophorus*, *Neolentiporus*, *Nothocastoreum*, *Notholepista*, *Ossicaulis*, *Paragyrodon*, *Paulisebacina*, *Phaeolepiota*, *Phaeomyces*, *Phallobata*, *Phylloboletellus*, *Piptoporus*, *Pirex*, *Polyozellus*, *Polypus*, *Porodisculus*, *Porpolomopsis*, *Protoxerula*, *Pseudohydnum*, *Pterulicium*, *Pulcherricium*, *Rhopalogaster*, *Richoniella*, *Royoungia*, *Sarcomyxa*, *Solioccasus*, *Sparsitubus*, *Sphagnurus*, *Stagnicola*, *Stromatoscypha*, *Sulzbacheromyces*, *Tephrocybella*, *Terana*, *Termiticola*, *Torrendia*, *Trametopsis*, *Tremellogaster*, *Tricholomella*, *Tsuchiyaea*, *Woldmaria*, *Xanthoporia*

Undersampled genera: *Clitocybe* s.l., *Clitopilus*, *Collybia*, *Ganoderma*, *Lachnella*, *Marasmiellus*, *Marasmius*, *Mycena*, *Peniophora*, *Russula*, *Tomentella*, *Tyromyces*

Trait independent diversification rate analyses - In BAMM analyses, all parameters converged to stationary values within the specified burn-in phase of the runs, based on diagnostic plots (Supplementary Fig. 9) and Geweke's diagnostics ($p > 0.05$). Despite the extremely long MCMC

chains (100 million generations), however, ESS values were moderate (< 200) for some of the parameters (Supplementary Table 7).

Detecting evolutionary rate shifts in Agaricomycetes evolution - After discarding the first 50 million generations as burn-in, we obtained 5001 samples from the posterior. Because virtually every posterior sample comprised a unique shift configuration (due to the size of the phylogeny being analyzed), we decided to focus on core shifts that are taxonomically and statistically consistent across >4 out of 10 chronograms, termed here congruent core shifts (for definition see the methods). After excluding non-congruent and mutually exclusive core shifts, we obtained 85 congruent core shifts (Supplementary Data 5). By calculating the cumulative posterior probability of the congruent core shifts as a function of generations we found that the posterior probabilities of each of the congruent core shifts were converged (Supplementary Fig. 9). Congruent core shifts were detected in several clades across the entire tree (Supplementary Data 5). We inferred congruent core shifts in the MRCA of many order-level clades, including the Tremellomycetes, the Dacrymycetes, the Cantharellales, the Sebacinales, the Auriculariales, the Hymenochaetales and Agaricales. In the Hymenochaetales, the shift was inferred in the MRCA of most species of the order, to the exception of the Repetobasidiaceae. Deeper in the tree, we detected rate shifts in the MRCA of each of the Phallomycetidae, Agaricomycetidae, the monophyletic group formed by Russulales, Polyporales, Thelephorales, Corticiales, Gloeophyllales and Jaapiales and the clade formed by Boletales, Amylocorticiales, Lepidostromatales and Atheliales. Most of the congruent core shifts were inferred in Agaricales (57). Also, all but 15 of them were associated with an increase in net diversification rate, indicating accelerated diversification.

Diversification rate changes through time - By analysing rates through time we found that net diversification rate started to increase between 197–163 mya in the Jurassic period (Fig. 2). To examine if this was a tree-wide pattern or was caused by a single or a few orders, we re-calculated rates through time by iteratively eliminating each of the orders and the Agaricomycetidae from the tree. This analysis showed that in most of the trees the signals did not disappear by excluding certain order or higher-level group (Fig. 2), suggesting that the Jurassic acceleration of diversification rate happened across the entire Agaricomycetes.
The main contributor to this pattern was speciation rate (Fig. 2). The acceleration of speciation rate was followed by an increase in extinction rate (195–125 Mya), consistent with the finding of potential mass extinction events (Fig. 2, Supplementary Fig. 6, Supplementary note 6).

Validation of BAMM estimates - Because BAMM's diversification estimates received criticism recently, we analyzed our data using a complementary approach as well. We found that the estimated evolutionary rates were congruent across the two methods and different settings (Supplementary Fig. 10, Supplementary Table 8; adjusted R squared: 0.41–0.60 and $p < 0.001$). The method-of-moments (MS) approach estimated lower diversification rate values relative to BAMM (Supplementary Fig. 10). In general, the MS estimates fit better to BAMM's diversification rates than to speciation rates. Furthermore, MS estimates obtained with crown ages generally fit better to BAMM data than those obtained with stem ages. The latter result was expected since BAMM estimates are based on only crown ages. Also, MS models without extinction rates ($\varepsilon = 0$) fit better to BAMM data than models with any extinction fractions (Supplementary Table 8). Altogether the two methods estimated similar mean diversification rates of clades, suggesting that our results are robust across different methods with different assumptions.

Supplementary Figures

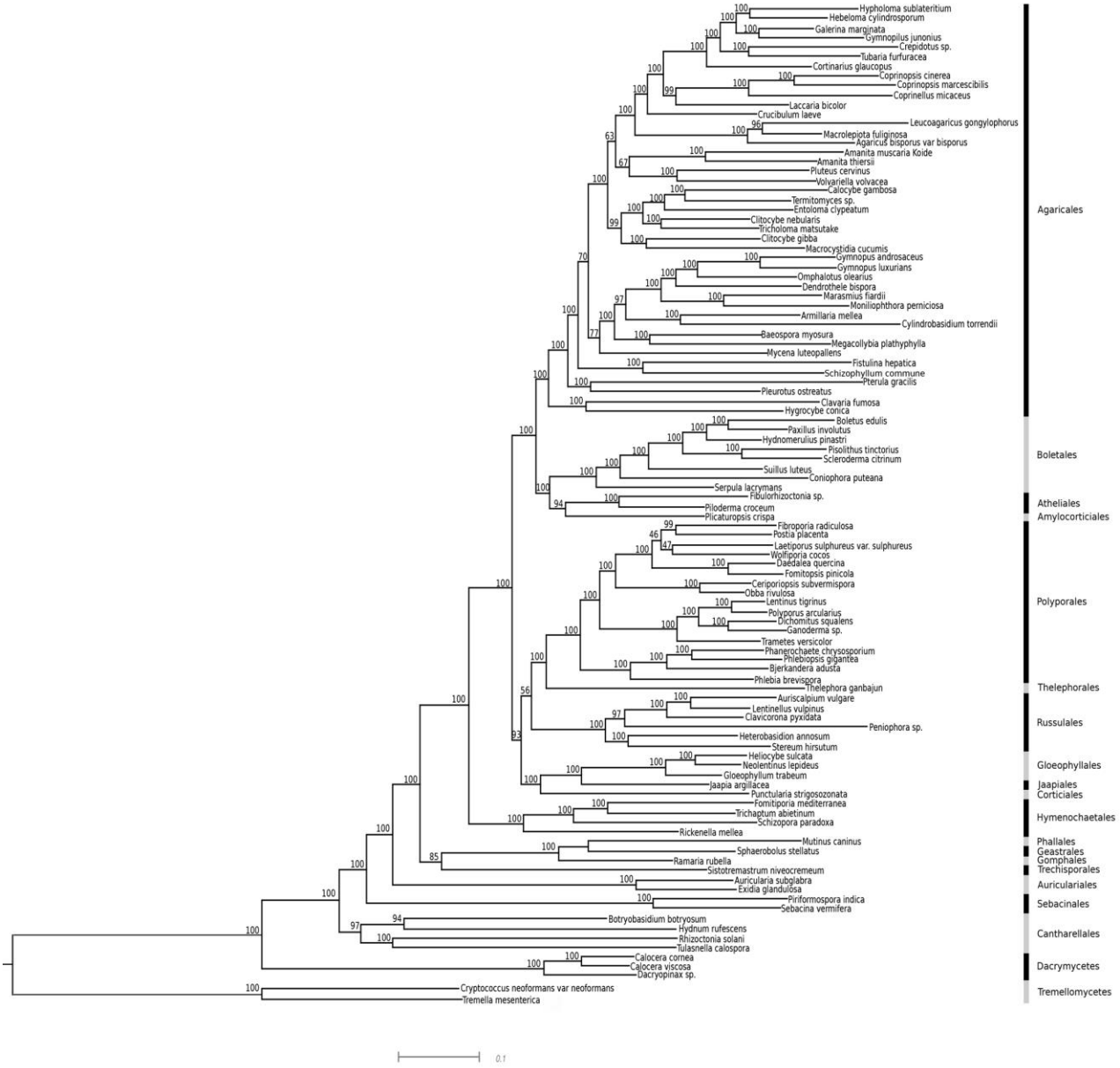

Supplementary Figure 1. Higher-level phylogenomic relationships of Agaricomycotina. Maximum-likelihood phylogenetic tree inferred from a supermatrix containing 141,951 amino acid sites partitioned into 650 genes from 104 genomes using RAxML under the PROTGAMMAWAG model. Numbers next to branches indicate the percent support from 100 nonparametric bootstraps. This phylogenomic tree was used as a topological constrain in the ML analysis of the 5284-species dataset.

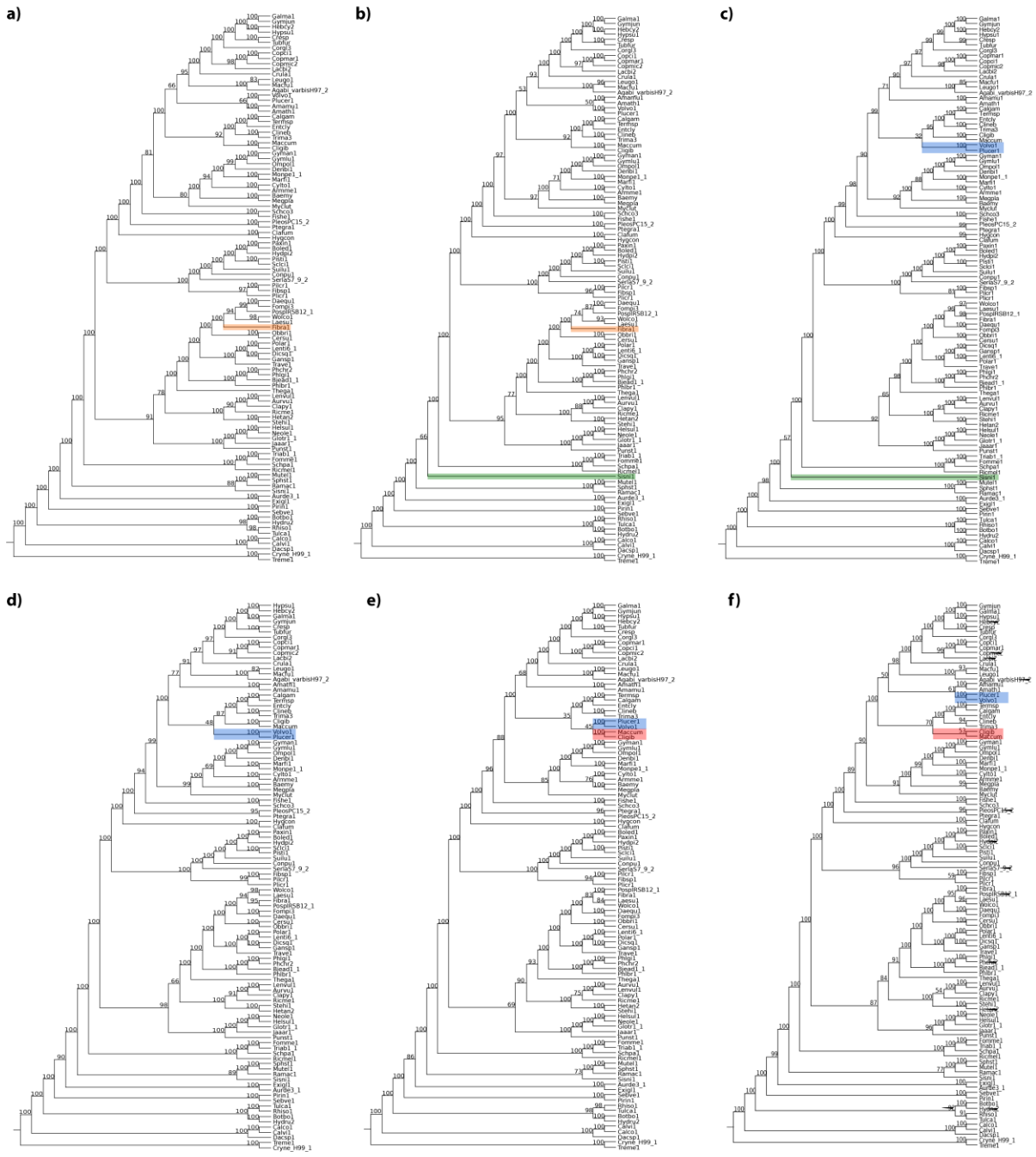

Supplementary Figure 2. Sensitivity analyses addressing the robustness of phylogenomic analyses. Maximum-likelihood trees inferred by progressively removing fast-evolving sites using Gblocks. Maximum Likelihood trees inferred from trimmed concatenated matrices containing 129.886 (A), 107.496 (B), 89.732 (C), 76.153 (D), 70.862 (E) and 63.309 (F) amino acid cites. Changes in topology affect the weekly supported branches shown by colored panels: *Fibroporia radiculosa* (Fibra1; orange) (A, B) and *Sistotremastrum niveocremeum* (Sisni1; green) (B, C), Pluteaceae (Plucer1, Volvo1; blue) (C-F) and Macrocystidiaceae (Cligib, Maccum; purple) (E,F).

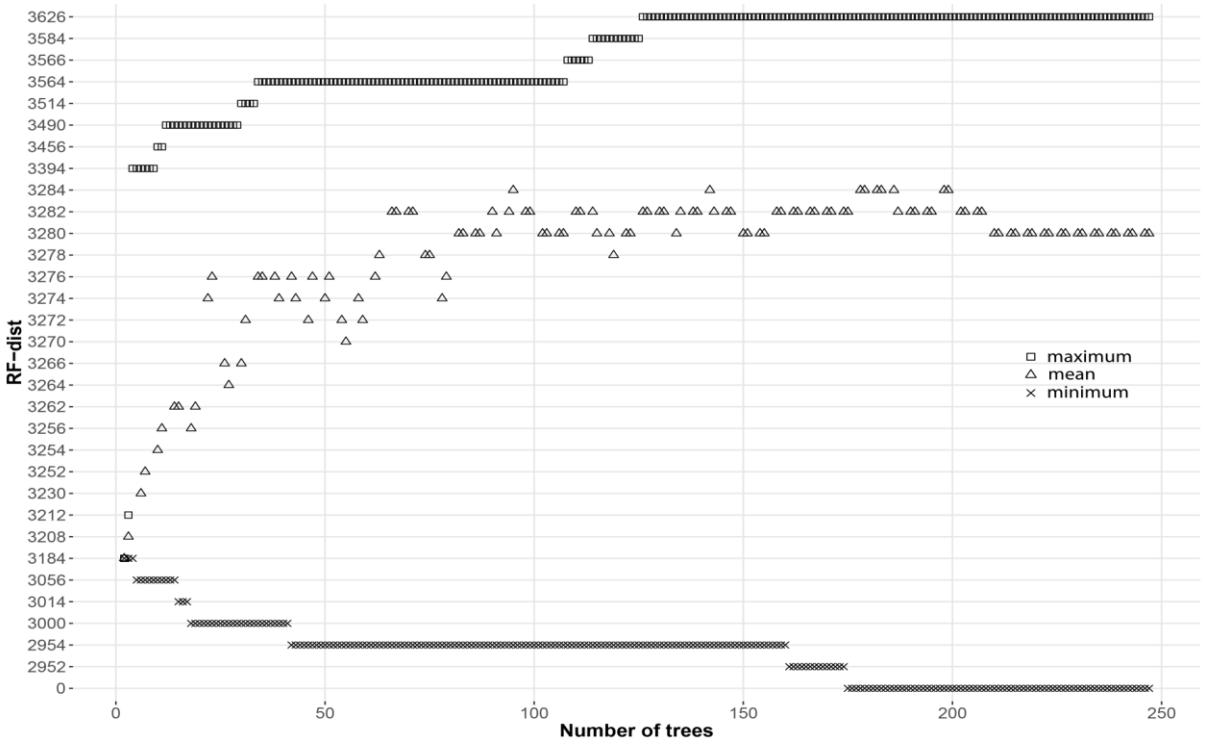

Supplementary Figure 3. The saturation of RF-distance values as a function of the number of ML trees. With increasing the number of trees the maximum, minimum and the average of pair-wise Robinson-Foulds distances are saturated.

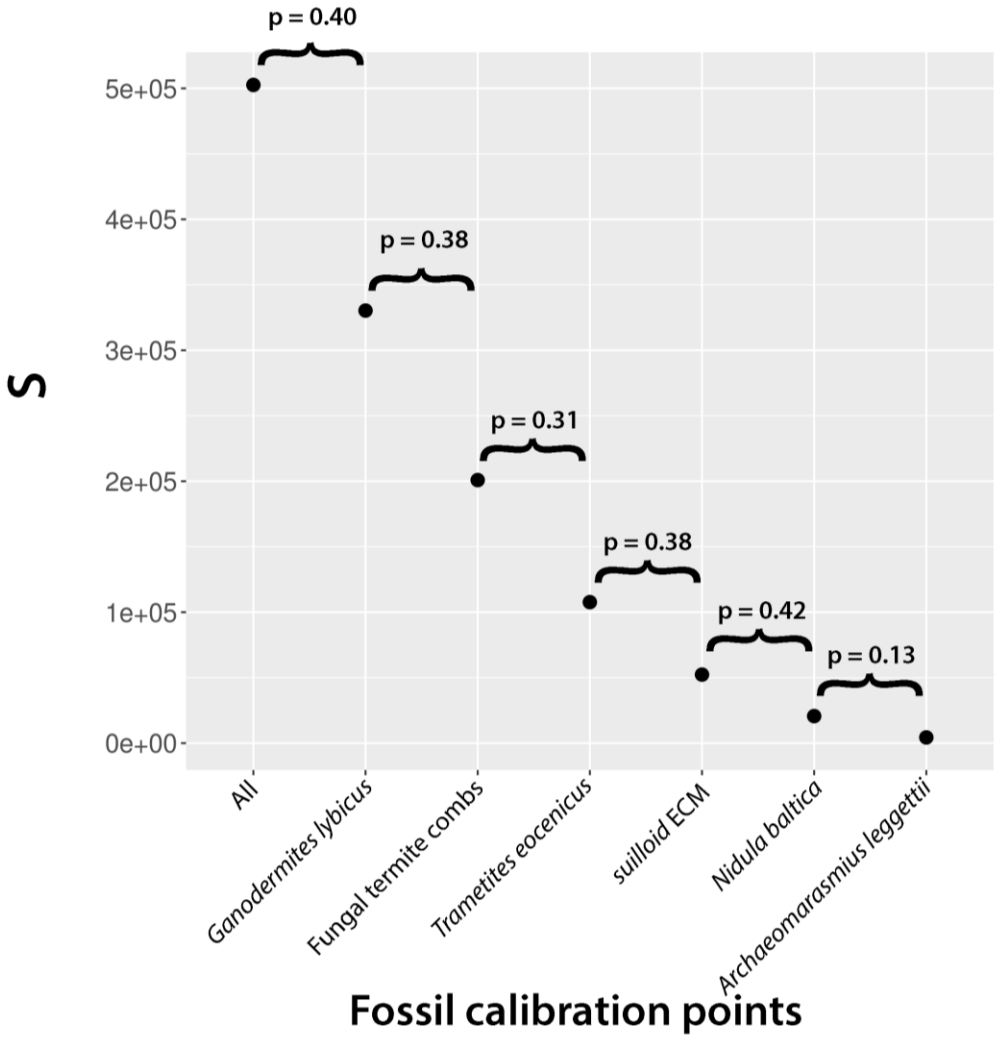

Supplementary Figure 4. The effects of removing fossil calibration points on the average squared deviation (*s*) between molecular and fossil age estimates for all calibration points. We conclude that fossil calibration points (listed in Supplementary Table 2) are not conflicting with each other because by removing a fossil calibration point *s* is decreased by an insignificant value, and there was no significant drop in the variance of *s* (one-tailed F-test, $p<0.05$) in any one comparison.

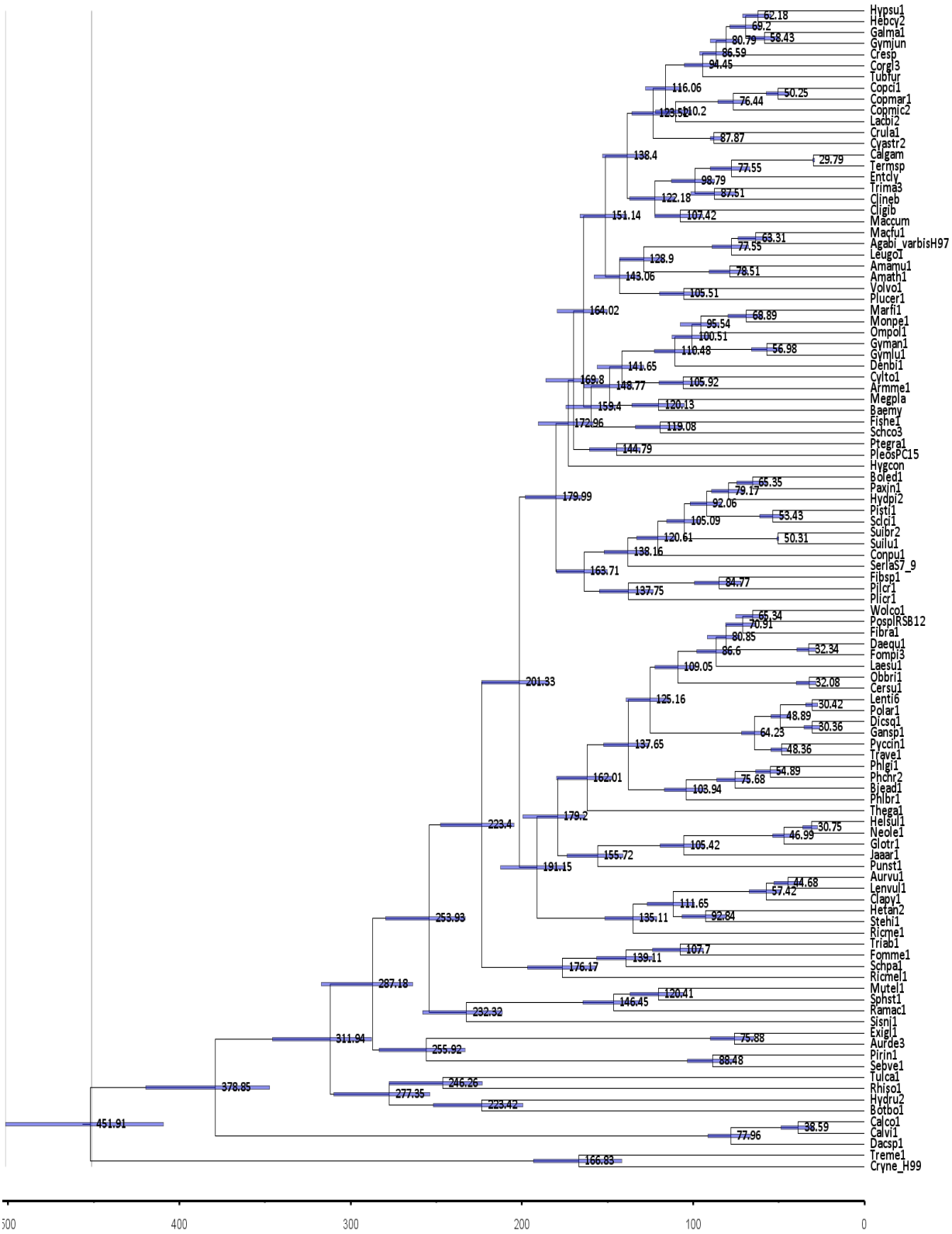

Supplementary Figure 5. Time calibrated chronogram inferred using mcmctree for the 105-species phylogenomic dataset. Numbers at nodes represent mean ages, bars are depict 95% highest posterior densities (HPD). For genome description see Supplementary Table 1.

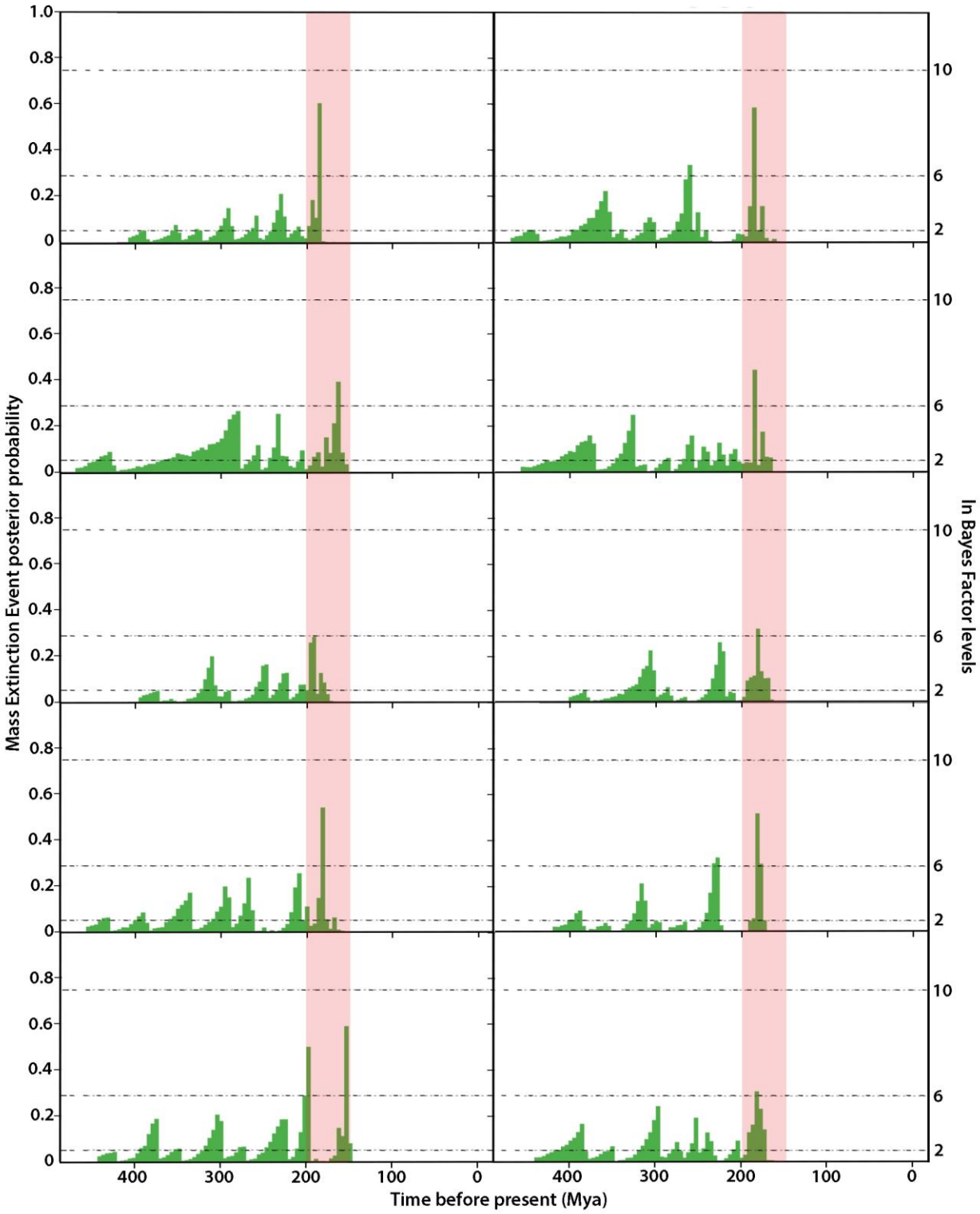

Supplementary Figure 6. Inferred mass extinction events. The left y-axis represents the posterior probability of a mass extinction event in a given time frame. Dashed lines indicate ln Bayes factor thresholds of significance. We considered ln Bayes factor>6 as strong support for an event (right y-axis). The 10 graphs represent the results for 10 analyzed chronograms. Shaded red region shows the interval of the Jurassic period.

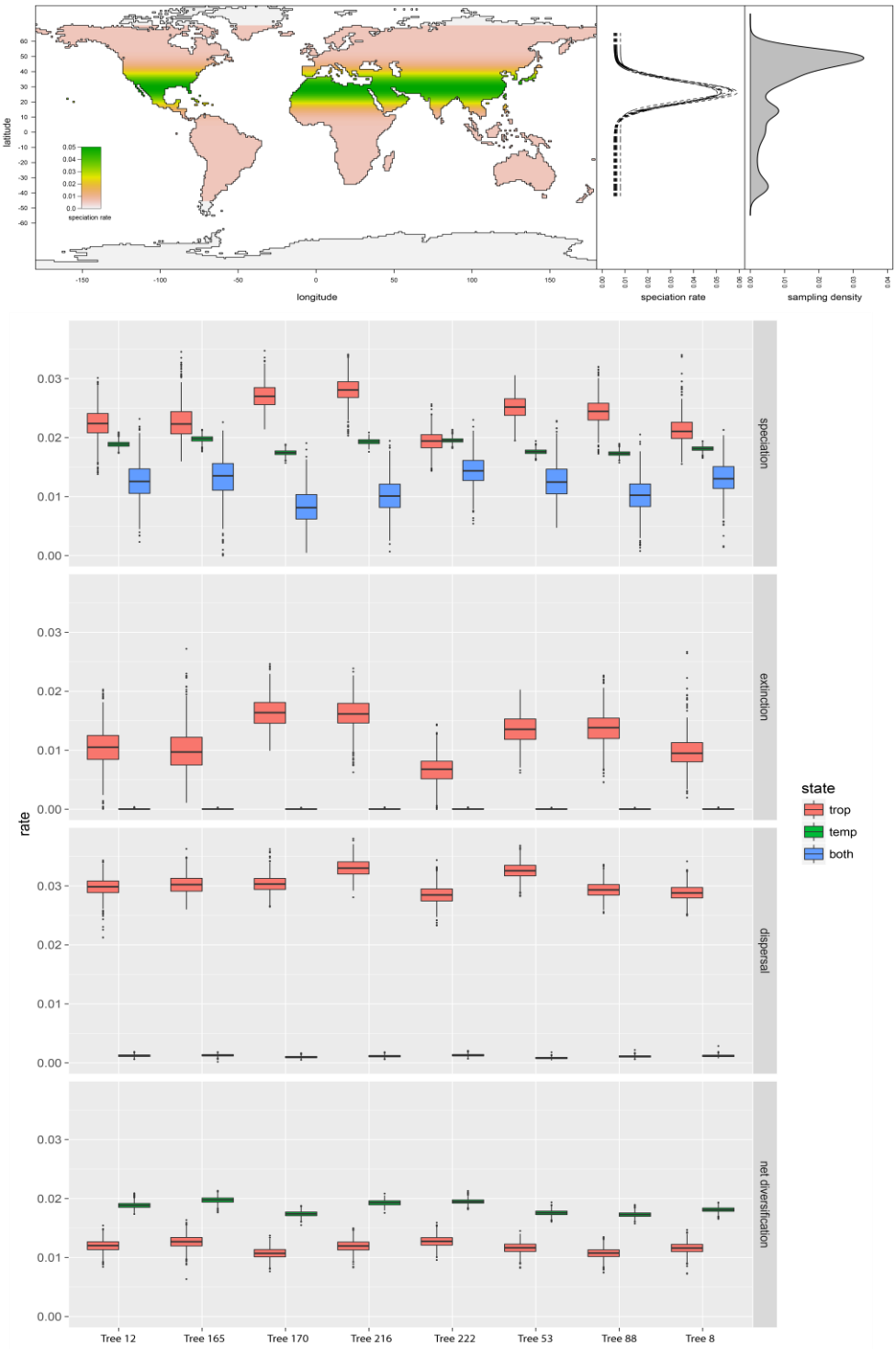

Supplementary Figure 7. Results of analyses of the latitudinal diversity gradient hypo-thesis. Upper panel shows the speciation rates in a 1 x 1 degree global map inferred under Quantitative State Speciation and Extinction (QuaSSE) model. On the right the distribution of the inferred speciation rates and the sampling density are shown along the latitudinal positions. Note that the sampling density doesn't overlap with the distribution of speciation rate. Lower panel shows the distribution of inferred rates using the Geographic State Speciation and Extinction (GeoSSE) model.

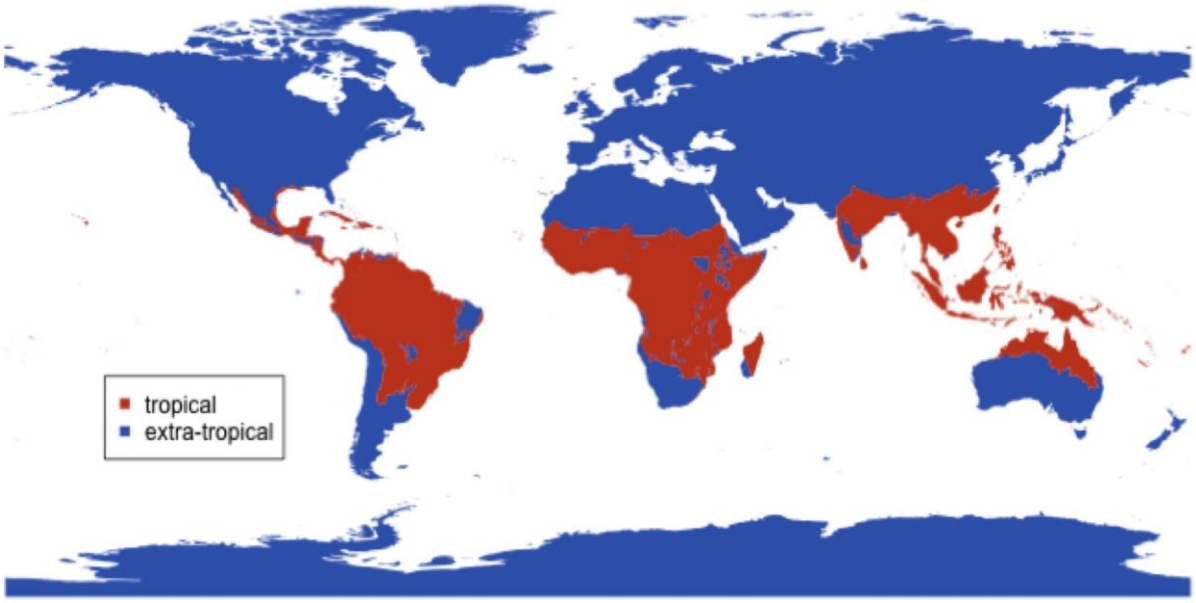

Supplementary Figure 8. The tropical and extra-tropical eco-regions

a)

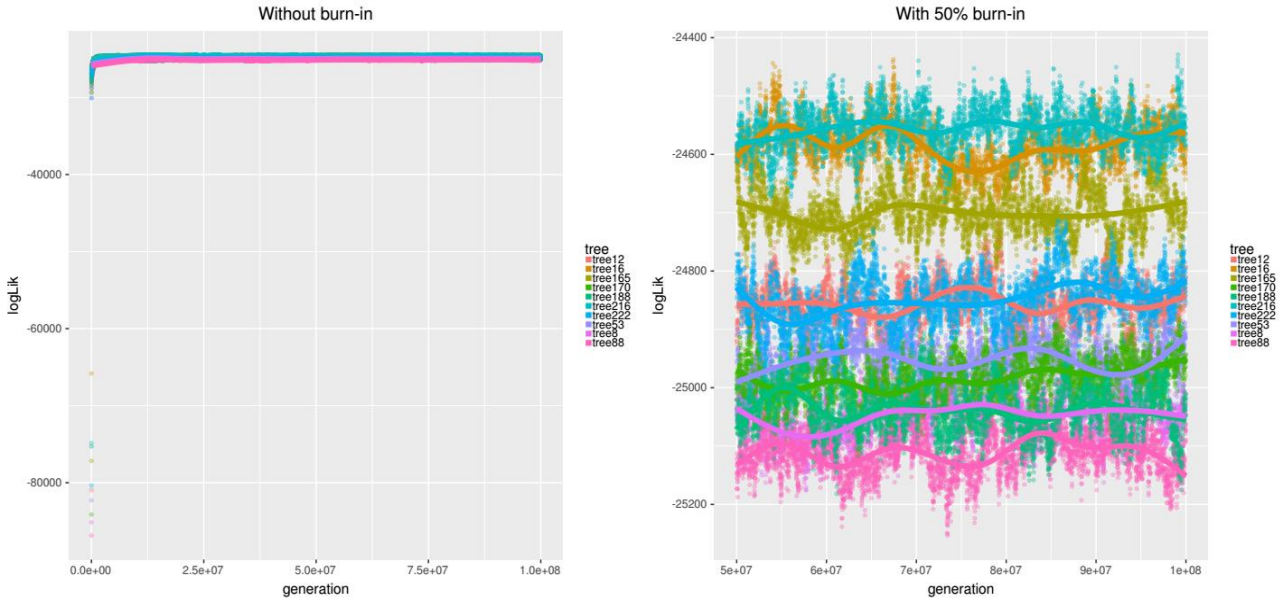

b)

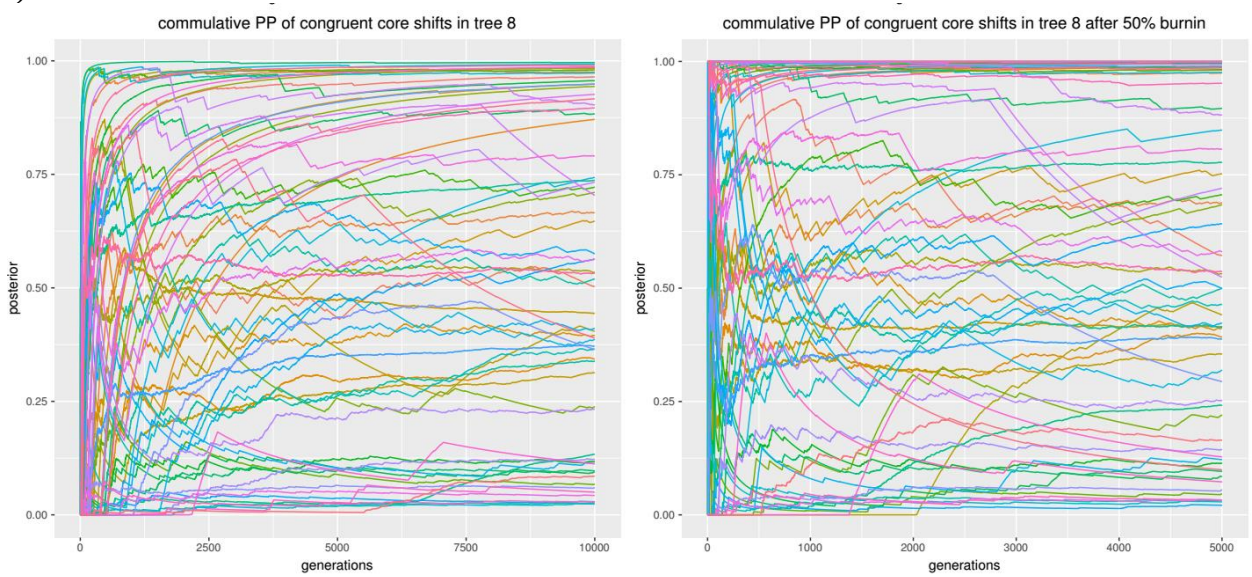

Supplementary Figure 9. a) The convergence of log likelihood values during the BAMM analyses. b) Cumulative posterior probability of congruent core shifts found in the BAMM analysis of tree 8. Left panel plots all samples obtained during the analysis; right panel shows only post-burn-in samples.

a)

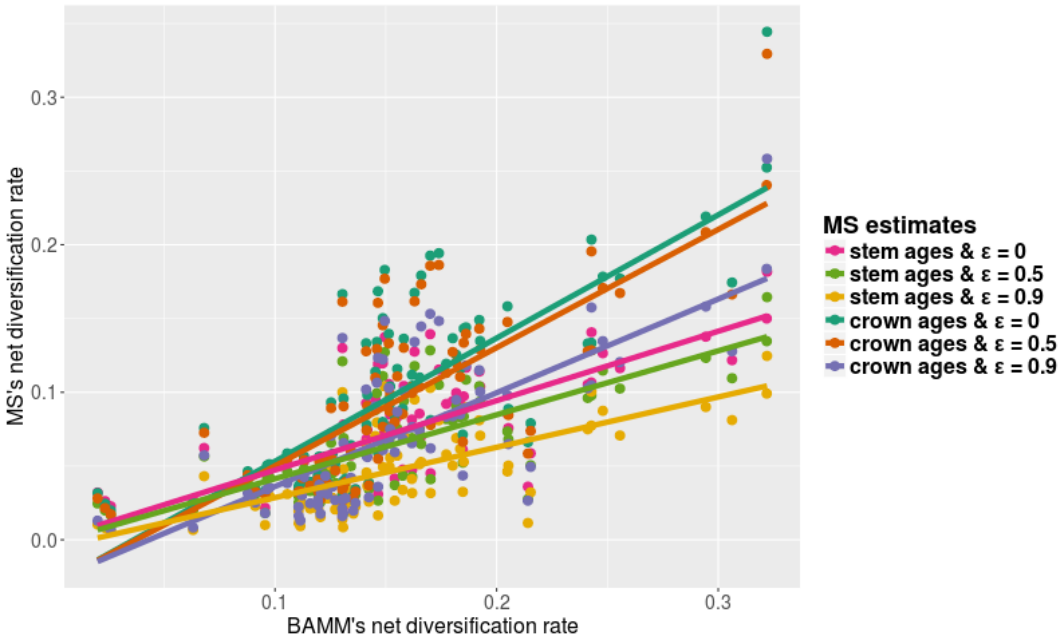

b)

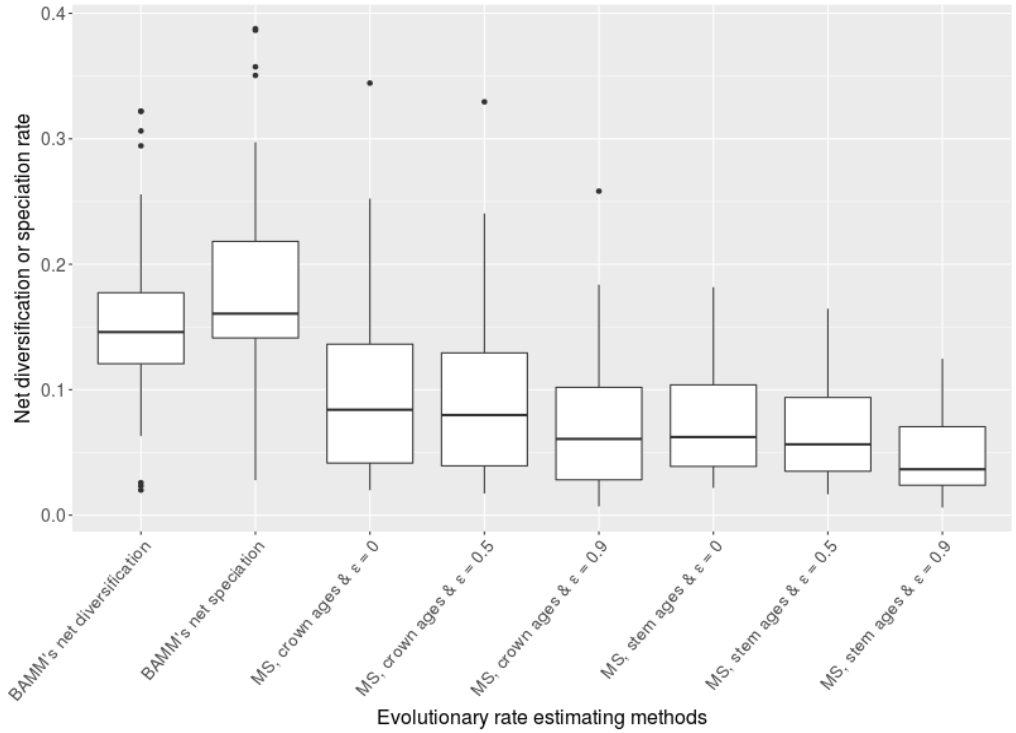

Supplementary Figure 10. a) Correlation between net diversification rate estimates by BAMM's and the MS method under various settings. ε = relative extinction rate. b) Comparison of results of BAMM and MS diversification rate estimates based on the average rates of 85 clades that subtend congruent core shifts. ε = relative extinction rate.

Supplementary Tables

Supplementary Table 1. Genomes used in this study. New genomes are in bold.

Species	Abbreviation	Order	Family	References
Agaricus bisporus var bisporus H97	Agabi_varbisH97_2	Agaricales	Agaricaceae	Morin et al.[25]
Amanita muscaria Koide	Amamu1	Agaricales	Amanitaceae	Kohler et al.[6]
Amanita thiersii	Amath1	Agaricales	Amanitaceae	Wolfe et al.[26]
Armillaria mellea	Armme1	Agaricales	Physalacriaceae	Collins et al.[27]
Auricularia subglabra	Aurde3_1	Auriculariales	Auriculariaceae	Floudas et al.[28]
Auriscalpium vulgare	Aurvu1	Russulales	Auriscalpiaceae	L. G. Nagy
Baeospora myosura	Baemy	Agaricales	Cyphellaceae*	B. T. M. Dentinger
Bjerkandera adusta	Bjead1_1	Polyporales	Meruliaceae (phlebioid clade[#])	Binder et al.[11]
Boletus edulis	Boled1	Boletales	Boletaceae	F. Martin
Botryobasidium botryosum	Botbo1	Cantharellales	Botryobasidiaceae	Riley et al.[29]
Calocera cornea	Calco1	Dacrymycetales	Dacrymycetaceae	Nagy et al.[5]
Calocybe gambosa	Calgam	Agaricales	Lyophyllaceae	B. T. M. Dentinger
Calocera viscosa	Calvi1	Dacrymycetales	Dacrymycetaceae	Nagy et al.[5]
Ceriporiopsis (Gelatoporia) subvermispora	Cersu1	Polyporales	gelatoporia clade[#]	Fernandez-Fueyo et al.[30]
Clavaria fumosa	Clafum	Agaricales	Clavariaceae	B. T. M. Dentinger
Clavicorona pyxidata (*Artomyces pyxidatus*)	Clapy1	Russulales	Auriscalpiaceae	L. G. Nagy
Clitocybe gibba (*Infundibulicybe gibba*)	Cligib	Agaricales	Tricholomataceae	B. T. M. Dentinger
Clitocybe nebularis	Clineb	Agaricales	Tricholomataceae	B. T. M. Dentinger
Coniophora puteana	Conpu1	Boletales	Coniophoraceae	Floudas et al.[7]
Coprinopsis cinerea	Copci1	Agaricales	Psathyrellaceae	Stajich et al.[31]
Coprinopsis marcescibilis	**Copmar1**	**Agaricales**	**Psathyrellaceae**	**This study**
Coprinellus micaceus	**Copmic2**	**Agaricales**	**Psathyrellaceae**	**This study**
Cortinarius glaucopus	Corgl3	Agaricales	Cortinariaceae *s str.**	F. Martin
Crepidotus sp.	Cresp	Agaricales	Crepidotaceae*	B. T. M. Dentinger
Crucibulum laeve	**Crula1**	**Agaricales**	**Nidulariaceae***	**This study**
Cryptococcus neoformans var neoformans	Cryne_H99_1	Tremellales	Tremellaceae	Janbon et al.[32]
Cylindrobasidium torrendii	Cylto1	Agaricales	Physalacriaceae	Floudas et al.[15]
Dacryopinax sp.	Dacsp1	Dacrymycetales	Dacrymycetaceae	Floudas et al.[7]
Daedalea quercina	Daequ1	Polyporales	Fomitopsidaceae (antrodia clade[#])	Nagy et al.[5]
Dendrothele bispora	**Denbi1**	**Agaricales**	**Corticiaceae**	**This study**
Dichomitus squalens	Dicsq1	Polyporales	Polyporaceae (core polyporoid clade[#])	Floudas et al.[7]
Entoloma clypeatum	Entcly	Agaricales	Entolomataceae	B. T. M. Dentinger
Exidia glandulosa	Exigl1	Auriculariales	Auriculariaceae	Nagy et al.[5]
Fibroporia radiculosa	Fibra1	Polyporales	Fomitopsidaceae (antrodia clade[#])	Tang et al.[33]
Fibulorhizoctonia sp.	Fibsp1	Atheliales	Atheliaceae	Nagy et al.[5]
Fistulina hepatica	Fishe1	Agaricales	Schizophyllaceae*	Floudas et al.[15]
Fomitiporia mediterranea	Fomme1	Hymenochaetales	Hymenochaetaceae	Floudas et al.[7]
Fomitopsis pinicola	Fompi3	Polyporales	Fomitopsidaceae (antrodia clade[#])	Floudas et al.[7]

Galerina marginata	Galma1	Agaricales	Hymenogastraceae	Riley et al.[29]
Ganoderma sp.	Gansp1	Polyporales	Ganodermataceae (core polyporoid clade[#])	Binder et al.[11]
Gloeophyllum trabeum	Glotr1_1	Gloeophyllales	Gloeophyllaceae	Floudas et al.[7]
Gymnopus androsaceus	Gyman1	Agaricales	Omphalotaceae	F. Martin
Gymnopilus junonius	Gymjun	Agaricales	Gymnopileae*	B. T. M. Dentinger
Gymnopus luxurians	Gymlu1	Agaricales	Omphalotaceae	Kohler et al.[6]
Hebeloma cylindrosporum	Hebcy2	Agaricales	Hymenogastraceae	Kohler et al.[6], Dore et al.[34]
Heliocybe sulcata	**Helsul1**	**Gloeophyllales**	**Gloeophyllaceae**	**This study**
Heterobasidion annosum	Hetan2	Russulales	Bondarzewiaceae	Olson et al.[35]
Hydnomerulius pinastri	Hydpi2	Boletales	Paxillaceae	Kohler et al.[6]
Hydnum rufescens	Hydru2	Cantharellales	Hydnaceae	Francis Martin
Hygrocybe conica	Hygcon	Agaricales	Hygrophoraceae	B. T. M. Dentinger
Hypholoma sublateritium	Hypsu1	Agaricales	Strophariaceae *s str.**	Kohler et al.[6]
Jaapia argillacea	Jaaar1	Jaapiales	Jaapiaceae	Riley et al.[29]
Laccaria bicolor	Lacbi2	Agaricales	Hydnangiaceae	Martin et al.[36]
Laetiporus sulphureus var. *sulphureus*	Laesu1	Polyporales	Fomitopsidaceae (antrodia clade[#])	Nagy et al.[5]
Lentinus tigrinus	Lenti6_1	Polyporales	Polyporaceae (core polyporoid clade[#])	D. Hibbett
Lentinellus vulpinus	Lenvul1	Russulales	Auriscalpiaceae	L. G. Nagy
Leucoagaricus gongylophorus	Leugo1	Agaricales	Agaricaceae	Aylward et al.[37]
Macrocystidia cucumis	Maccum	Agaricales	Macrocystidiaceae*	B. T. M. Dentinger
Macrolepiota fuliginosa	Macfu1	Agaricales	Agaricaceae	F. Martin
Marasmius fiardii	Marfi1	Agaricales	Marasmiaceae	F. Martin
Megacollybia plathyphylla	Megpla	Agaricales	hydropoid clade*	B. T. M. Dentinger
Moniliophthora perniciosa	Monpe1_1	Agaricales	Marasmiaceae	Mondego et al.[38]
Mutinus caninus	Mutel1	Phallales	Phallaceae	P. Crous
Mycena luteopallens	Myclut	Agaricales	Mycenaceae	B. T. M. Dentinger
Neolentinus lepideus	Neole1	Gloeophyllales	Gloeophyllaceae	Nagy et al.[5]
Obba rivulosa	Obbri1	Polyporales	gelatoporia clade[#]	Miettinen et al.[39]
Omphalotus olearius	Ompol1	Agaricales	Omphalotaceae	Wawrzyn et al.[40]
Paxillus involutus	Paxin1	Boletales	Paxillaceae	Kohler et al.[6]
***Peniophora* sp.**	**Ricme1**	**Russulales**	**Peniophoraceae**	**Nagy et al.**[5]
Phanerochaete chrysosporium	Phchr2	Polyporales	Phanerochaetaceae (phlebioid clade[#])	Ohm et al.[41]
Phlebia brevispora	Phlbr1	Polyporales	Phanerochaetaceae (phlebioid clade[#])	Binder et al.[11]
Phlebiopsis gigantea	Phlgi1	Polyporales	Phanerochaetaceae (phlebioid clade[#)]	Hori et al.[42]
Piloderma croceum	Pilcr1	Atheliales	Atheliaceae	Kohler et al.[6]
Piriformospora indica	Pirin1	Sebacinales		Zuccaro et al.[43]
Pisolithus tinctorius	Pisti1	Boletales	Sclerodermataceae	Kohler et al.[6]
Pleurotus ostreatus	PleosPC15_2	Agaricales	Pleurotaceae	Riley et al.[29], Castanera et al.[44], Alfaro et al.[45]
Plicaturopsis crispa	Plicr1	Amylocorticiales	Amylocorticiaceae	Kohler et al.[6]
Pluteus cervinus	**Plucer1**	**Agaricales**	**Pluteaceae**	**This study**
Polyporus arcularius	**Polar1**	**Polyporales**	**Polyporaceae (core polyporoid clade[#])**	**This study**

Postia placenta	PosplRSB12_1	Polyporales	Polyporaceae(antrodia clade[#])	Martinez et al.[46]
Pterula gracilis	**Ptegra1**	**Agaricales**	**Pterulaceae**	**This study**
Punctularia strigosozonata	Punst1	Corticiales	Punctulariaceae	Floudas et al.[7]
Ramaria rubella	Ramac1	Gomphales	Gomphaceae	F. Martin
Rhizoctonia solani	Rhiso1	Cantharellales	Ceratobasidiaceae	Wibberg et al.[47]
Rickenella mellea	Ricmel1	Hymenochaetales	Repetobasidiaceae	L. G. Nagy
Schizophyllum commune	Schco3	Agaricales	Schizophyllaceae	J. Stephen Horton
Schizopora paradoxa	Schpa1	Hymenochaetales	Schizoporaceae	Min et al.[48]
Scleroderma citrinum	Sclci1	Boletales	Sclerodermataceae	Kohler et al.[6]
Sebacina vermifera	Sebve1	Sebacinales		Kohler et al.[6]
Serpula lacrymans	SerlaS7_9_2	Boletales	Serpulaceae	Eastwood et al.[49]
Sistotremastrum niveocremeum	Sisni1	Trechisporales	Hydnodontaceae	Nagy et al.[5]
Sphaerobolus stellatus	Sphst1	Geastrales	Geastraceae	Kohler et al.[6]
Stereum hirsutum	Stehi1	Russulales	Stereaceae	Floudas et al.[7]
Suillus luteus	Suilu1	Boletales	Suillaceae	Kohler et al.[6]
Termitomyces sp.	Termsp	Agaricales	Lyophyllaceae	B. T. M. Dentinger
Thelephora ganbajun	Thega1	Thelephorales	Telephoraceae	P. Wang
Trametes versicolor	Trave1	Polyporales	Polyporaceae (core polyporoid clade[#])	Floudas et al.[7]
Tremella mesenterica Fries	Treme1	Tremellales	Tremellaceae	Floudas et al.[7]
Trichaptum abietinum	Triab1_1	Hymenochaetales		L. G. Nagy
Tricholoma matsutake	Trima3	Agaricales	Tricholomataceae	F. Martin
Tubaria furfuracea	Tubfur	Agaricales	Tubariae*	B. T. M. Dentinger
Tulasnella calospora	Tulca1	Cantharellales	Tulsanellaceae	Kohler et. al[6]
Volvariella volvacea	Volvo1	Agaricales	Pluteaceae	Bao et al.[50]
Wolfiporia cocos	Wolco1	Polyporales	Polyporaceae (antrodia clade[#])	Floudas et al.[7]

*Classification based on Matheny et al.[14]
Binder et al.[11]

Supplementary Table 2. Nine calibration points used in molecular dating of phylogenetic trees. An age constraint was further applied to the root because molecular age estimation methods generally poorly resolve root ages. All calibration points define the crown node of each group listed here.

Fossil	**Calibration point**	**Mininum Age (myr)**	**Maximum Age (myr)**	**Reference**
Quatsinoporites cranhamii	Hymenochaetales	127	250	Smith et al.[51]
Ganodermites lybicus	Ganoderma	18	50	Fleischmann et al.[52]
Archaemarasmius legettii	marasmioid clade	92	180	Hibbett et al.[53]
Palaeoagaricites antiquus	Agaricales	105	210	Poinar & Buckley[54]
Nidula baltica	Nidulariaceae	45	90	Poinar[55]
Suilloid ECM	Suillaceae	50	100	Lepage et al.[56]
Fungal termite combs	Termitomyces	7	30	Duringer et al.[57]
Trametites eocenicus	Trametes	45	90	Knobloch & Kotlaba[58]
	Root	300	600	

Supplementary Table 3. Results of MCMC analyses under models with and without mass extinction events. The null model (M_0) was a constant-rate birth-death CoMET model with mass extinction events allowed and the alternative model (M_1) was the same as M_0 but without a mass extinction event. Bayes factors were calculated from the marginal likelihoods of the two models, using stepping stone simulation.

Tree analyzed	Marginal log likelihood values		Bayes Factor
	Mass extinction	No mass extinction	
8	-24116	-24128	23
12	-23930	-23947	34
16	-23543	-23554	21
53	-23826	-23838	25
88	-24032	-24043	22
165	-23638	-23648	21
170	-24049	-24065	31
188	-24058	-24071	26
216	-23480	-23494	27
222	-23937	-23951	27

Supplementary Table 4. Convergence statistics of numerical parameters in rjMCMC analyses of CoMET models.

Trees	**log likelihood**			**# of Speciation rate shifts**			**# of Extinction rate shifts**			**# of Mass extinction events**		
	Mean	ESS	Geweke statistics	Mean	ESS	Geweke statistics	Mean	ESS	Geweke statistics	Mean	ESS	Geweke statistics
Tree 8	-23844	2108	sig.	30	2224	non sig.	29	1806	non sig.	3.4	2275	non sig.
Tree 12	-23646	2251	non sig.	30	2251	non sig.	27	1842	non sig.	4.4	2251	non sig.
Tree 16	-23241	2119	non sig.	30	2251	non sig.	30	1797	non sig.	5.4	2295	non sig.
Tree 53	-23449	2251	non sig.	30	2103	non sig.	28	1733	non sig.	4.6	1778	non sig.
Tree 88	-23638	922	sig.	29	2251	non sig.	28	1354	non sig.	3.2	2185	non sig.
Tree 165	-23301	2251	sig.	30	2251	non sig.	27	1541	non sig.	3.7	2251	non sig.
Tree 170	-23726	2251	sig.	30	2251	non sig.	28	1363	non sig.	4.4	1960	non sig.
Tree 188	-23685	1113	sig.	30	2251	sig.	28	2072	non sig.	3.7	2251	non sig.
Tree 216	-23106	2251	sig.	30	2251	non sig.	29	1895	non sig.	5.1	2251	non sig.
Tree 222	-23671	1641	sig.	30	2251	non sig.	28	1848	non sig.	4.3	2251	non sig.

Supplementary Table 5. QuaSSE model fit. Values are averaged across 10 trees. dAIC is the AIC differences between the best and other models. lnL is the ln-likelihood of the given model.

Model	Df	lnL	AIC	dAIC	p-value
Constant speciation and extinction	3	-50732.2	101470.5	949.8	--
Gaussian speciation and const. extinction	**6**	**-50254.3**	**100520.7**	**0**	**<2e-16 *****
Linear speciation and const. extinction	4	-50732.1	101472.4	951.7	0.59
Const. speciation and linear extinction	4	-50732.2	101472.4	951.7	0.84
Const. speciation and Gaussian extinction	6	-50732.1	101476.2	955.5	0.93

Supplementary Table 6. GeoSSE model fit. Values are averaged across 10 trees. dAIC is the AIC differences between the best and other models. lnL is the ln-likelihood of the given model.

Model	Df	lnL	AIC	dAIC	p-value
full	**7**	**-28232.0**	**56478.0**	**0**	**--**
Equal speciation	5	-28294.7	56599.4	121.4	<2e-16 ***
Equal extinction	6	-28243.7	56499.4	21.4	0.001 ****
Equal dispersal	6	-28348.4	56708.9	230.8	<2e-16 ***

Supplementary Table 7. ESS values and Geweke's statistics of different parameters summarized across BAMM analyses of ten chronograms.

Statistics	**Statistical measures**	**number of shifts**	**Log prior**	**Log Likelihood**	**eventRate**	**acceptRate**
ESS	**min**	83	73	56	181	1616
	mean	140	143	83	265	2146
	max	186	185	121	330	2818
Geweke's statistics	**# of trees p > 0.05**	7	7	9	7	7

Supplementary Table 8. The results of linear regression analyses where the dependent variable was BAMM's net diversification or net speciation rate and the explanatory variable was net diversification rate inferred using the MS approach. ε = relative extinction rate.

MS estimates as explanatory variables	Statistics based on BAMM's net diversification rate (dependent variable)		Statistics based on BAMM's speciation rate (dependent variable)	
	Adjusted R^2	P-value	Adjusted R^2	P-value
stem ages & ε = 0	0.51	9.18E-15	0.45	9.17E-13
stem ages & ε = 0.5	0.50	2.42E-14	0.45	1.63E-12
stem ages & ε = 0.9	0.45	1.26E-12	0.41	2.47E-11
crown ages & ε = 0	0.60	2.68E-18	0.53	2.28E-15
crown ages & ε = 0.5	0.59	4.87E-18	0.52	3.27E-15
crown ages & ε = 0.9	0.55	3.48E-16	0.49	5.51E-14

Legends for supplementary data

Supplementary Data 1. (Separate file).
Data matrices of GenBank accession numbers of newly sequenced taxa, character states used for analyses of character evolution and taxon sampling statistics used in this study. The GenBank accession numbers are depicted for LSU sequences of 1213 newly sequenced species. The character state coding of cap presence/absence, fruiting body morphology, substrate preference and geographic distributions for 5,284 species is given.

Supplementary Data 2. (Separate file). Comparison of results of different molecular dating analyses. The inferred ages of seven clades (Agaricales, Boletales, Agaricomycetidae, Agaricomycetes, most recent common ancestor of Agaricomycetes and Dacrymycetes, Agaricomycotina) were compared with the estimates of two previous studies and five analyses of the present study (three methods r8s, mcmctree and a 2-stage Bayesian approach and three calibration schemes) to assess the impact of alternative placements of fossil calibration points.

Supplementary Data 3. (Separate file). Transition rate matrices of ancestral character state reconstruction (ASR) analyses and results of the ASR of fungal substrate preference.

Supplementary Data 4. (Separate file). Speciation, extinction and diversification rates through time obtained by iteratively removing orders and higher level clades from the phylogeny. Different colors represent the ten chronograms analyzed. Lines are median rates and color density denotes the 80% Bayesian credible regions on the distribution of rates. For each plot, the upper row (A) shows the rates calculated for the given clade, the lower (B) shows rates calculated for the entire tree, with the given clade deleted.

Supplementary Data 5. (Separate file). List of highly supported core shifts that are congruent across multiple trees. Statistics of the shifts (Posterior probability, Prior to posterior odds ratio, Speciation rate change etc.) are given. Mean values are the average across the trees containing a core shift.

Supplementary Data 6. (Separate file). Lineages through time (LTT) plots for the clades containing highly supported core shifts. LTT plots were generated from branches subtending a congruent core shift with the ltt.plot function in the R package ape v.4.1. Dashed red line represents the log linear (exponential) change of the number of lineages based on the extant species number. If the slope of the inferred changes in lineage number is higher or lower than that of the dashed red line, the number of lineages increased faster or slower than it is expected.

Supplementary Data 7. (Separate file). Parameters and detailed results of BayesTraits and BiSSE analyses. The mean and the variance of the estimated transition rates are given for the Maximum Likelihood and Bayesian MCMC analyses of BayesTraits and BiSSE analyses. Furthermore, the hyperprior intervals are given for Bayesian analyses in BayesTraits. Results of the model tests are also included: log likelihood values, bayes factors, likelihood ratio tests.

References

1. Rodréguez-Ezpeleta, N. *et al.* Detecting and overcoming systematic Errors in genome-scale phylogenies. *Syst. Biol.* **56,** 389–399 (2007).
2. Dentinger, B. T. M. *et al.* Tales from the crypt: Genome mining from fungarium specimens improves resolution of the mushroom tree of life. *Biol. J. Linn. Soc.* **117,** 11–32 (2016).
3. Zhao, R.-L. *et al.* A six-gene phylogenetic overview of Basidiomycota and allied phyla with estimated divergence times of higher taxa and a phyloproteomics perspective. *Fungal Divers.* **84,** 43–74 (2017).
4. Hibbett, D. S. A phylogenetic overview of the Agaricomycotina. *Mycologia* **98,** 917–925 (2006).
5. Nagy, L. G. *et al.* Comparative genomics of early-diverging mushroom-forming fungi provides insights into the origins of lignocellulose decay capabilities. *Mol. Biol. Evol.* **33,** 959–970 (2016).
6. Kohler, A. *et al.* Convergent losses of decay mechanisms and rapid turnover of symbiosis genes in mycorrhizal mutualists. *Nat. Genet.* **47,** 410–415 (2015).
7. Floudas, D. *et al.* The Paleozoic Origin of Enzymatic Lignin Decomposition Reconstructed from 31 Fungal Genomes. *Science (80-.).* **336,** 1715–1719 (2012).
8. Hibbett, D. S. *et al.* in *Systematics and Evolution* 373–429 (Springer Berlin Heidelberg, 2014). doi:10.1007/978-3-642-55318-9_14
9. Matheny, B. P. *et al.* Contributions of rpb2 and tef1 to the phylogeny of mushrooms and allies (Basidiomycota, Fungi). *Mol. Phylogenet. Evol.* **43,** 430–451 (2007).
10. Binder, M., Larsson, K.-H., Matheny, P. B. & Hibbett, D. S. Amylocorticiales ord. nov. and Jaapiales ord. nov.: Early diverging clades of Agaricomycetidae dominated by corticioid forms. *Mycologia* **102,** 865–880 (2010).
11. Binder, M. *et al.* Phylogenetic and phylogenomic overview of the Polyporales. *Mycologia* **105,** 1350–1373 (2013).
12. Binder, M. *et al.* The phylogenetic distribution of resupinate forms across the major clades of mushroom-forming fungi (Homobasidiomycetes). *Syst. Biodivers.* **3,** 113–157 (2005).
13. Justo, A. *et al.* A revised family-level classification of the Polyporales (Basidiomycota). *Fungal Biol.* **121,** 798–824 (2017).
14. Matheny, P. B. *et al.* Major clades of Agaricales: a multilocus phylogenetic overview. *Mycologia* **98,** 982–995 (2006).
15. Floudas, D. *et al.* Evolution of novel wood decay mechanisms in Agaricales revealed by the genome sequences of Fistulina hepatica and Cylindrobasidium torrendii. *Fungal Genet. Biol.* **76,** 78–92 (2015).
16. Nagy, L. G. *et al.* Latent homology and convergent regulatory evolution underlies the repeated emergence of yeasts. *Nat. Commun.* **5,** 4471 (2014).
17. Binder, M. & Hibbett, D. S. Molecular systematics and biological diversification of Boletales. *Mycologia* **98,** 971–981 (2006).
18. Gnerre, S. *et al.* High-quality draft assemblies of mammalian genomes from massively parallel sequence data. *Proc. Natl. Acad. Sci.* **108,** 1513–1518 (2011).
19. Martin, J. *et al.* Rnnotator: an automated de novo transcriptome assembly pipeline from stranded RNA-Seq reads. *BMC Genomics* **11,** 663 (2010).
20. Grigoriev, I. V *et al.* MycoCosm portal: Gearing up for 1000 fungal genomes. *Nucleic Acids Res.* **42,** (2014).

21. Lidgard, S. & Crane, P. R. Quantitative analyses of the early angiosperm radiation. *Nature* **331,** 344–346 (1988).
22. Smith, J. F. *et al.* The Emergence of Earliest Angiosperms May be Earlier than Fossil Evidence Indicates. *Syst. Bot.* **42,** 1–13 (2017).
23. Lu, Y., Ran, J., Guo, D., Yang, Z. & Wang, X. Phylogeny and Divergence Times of Gymnosperms Inferred from Single-Copy Nuclear Genes. *PLoS One* **9,** 1–15 (2014).
24. Goldberg, E. E., Lancaster, L. T. & Ree, R. H. Phylogenetic Inference of Reciprocal Effects between Geographic Range Evolution and Diversification. *Syst. Biol.* **60,** 451–465 (2011).
25. Morin, E. *et al.* Genome sequence of the button mushroom Agaricus bisporus reveals mechanisms governing adaptation to a humic-rich ecological niche. *Proc. Natl. Acad. Sci.* **109,** 17501–17506 (2012).
26. Wolfe, B. E., Kuo, M. & Pringle, A. *Amanita thiersii* is a saprotrophic fungus expanding its range in the United States. *Mycologia* **104,** 22–33 (2012).
27. Collins, C. *et al.* Genomic and proteomic dissection of the ubiquitous plant pathogen, armillaria mellea: Toward a new infection model system. *J. Proteome Res.* **12,** 2552–2570 (2013).
28. Floudas, D. *et al.* The Paleozoic origin of enzymatic lignin decomposition reconstructed from 31 fungal genomes. *Science* **336,** 1715–9 (2012).
29. Riley, R. *et al.* Extensive sampling of basidiomycete genomes demonstrates inadequacy of the white-rot/brown-rot paradigm for wood decay fungi. *Proc. Natl. Acad. Sci.* **111,** 9923–9928 (2014).
30. Fernandez-Fueyo, E. *et al.* Comparative genomics of Ceriporiopsis subvermispora and Phanerochaete chrysosporium provide insight into selective ligninolysis. *Proc. Natl. Acad. Sci.* **109,** 5458–5463 (2012).
31. Stajich, J. E. *et al.* Insights into evolution of multicellular fungi from the assembled chromosomes of the mushroom Coprinopsis cinerea (Coprinus cinereus). *Proc. Natl. Acad. Sci. U. S. A.* **107,** 11889–11894 (2010).
32. Janbon, G. *et al.* Analysis of the Genome and Transcriptome of Cryptococcus neoformans var. grubii Reveals Complex RNA Expression and Microevolution Leading to Virulence Attenuation. *PLoS Genet.* **10,** e1004261 (2014).
33. Tang, J. D. *et al.* Short-read sequencing for genomic analysis of the brown rot fungus Fibroporia radiculosa. *Appl. Environ. Microbiol.* **78,** 2272–2281 (2012).
34. Doré, J. *et al.* Comparative genomics, proteomics and transcriptomics give new insight into the exoproteome of the basidiomycete Hebeloma cylindrosporum and its involvement in ectomycorrhizal symbiosis. *New Phytol.* **208,** 1169–1187 (2015).
35. Olson, Å. *et al.* Insight into trade-off between wood decay and parasitism from the genome of a fungal forest pathogen. *New Phytol.* **194,** 1001–1013 (2012).
36. Martin, F. *et al.* The genome of Laccaria bicolor provides insights into mycorrhizal symbiosis. *Nature* **452,** 88–92 (2008).
37. Aylward, F. O. *et al.* Leucoagaricus gongylophorus Produces Diverse Enzymes for the Degradation of Recalcitrant Plant Polymers in Leaf-Cutter Ant Fungus Gardens. *Appl. Environ. Microbiol.* **79,** 3770–3778 (2013).
38. Mondego, J. M. C. *et al.* A genome survey of Moniliophthora perniciosa gives new insights into Witches' Broom Disease of cacao. *BMC Genomics* **9,** (2008).
39. Miettinen, O. *et al.* Draft Genome Sequence of the White-Rot Fungus Obba rivulosa 3A-

2. *Genome Announc.* **4,** 00976-16 (2016).
40. Wawrzyn, G. T., Quin, M. B., Choudhary, S., López-Gallego, F. & Schmidt-Dannert, C. Draft Genome of Omphalotus olearius Provides a Predictive Framework for Sesquiterpenoid Natural Product Biosynthesis in Basidiomycota. *Chem. Biol.* **19,** 772–783 (2012).
41. Ohm, R. A. *et al.* Genomics of wood-degrading fungi. *Fungal Genet. Biol.* **72,** 82–90 (2014).
42. Hori, C. *et al.* Analysis of the Phlebiopsis gigantea Genome, Transcriptome and Secretome Provides Insight into Its Pioneer Colonization Strategies of Wood. *PLoS Genet.* **10,** (2014).
43. Zuccaro, A. *et al.* Endophytic life strategies decoded by genome and transcriptome analyses of the mutualistic root symbiont Piriformospora indica. *PLoS Pathog.* **7,** (2011).
44. Castanera, R. *et al.* Transposable Elements versus the Fungal Genome: Impact on Whole-Genome Architecture and Transcriptional Profiles. *PLoS Genet.* **12,** 1–27 (2016).
45. Alfaro, M. *et al.* Comparative and transcriptional analysis of the predicted secretome in the lignocellulose-degrading basidiomycete fungus Pleurotus ostreatus. *Environ. Microbiol.* **18,** 4710–4726 (2016).
46. Martinez, D. *et al.* Genome, transcriptome, and secretome analysis of wood decay fungus *Postia placenta*supports unique mechanisms of lignocellulose conversion. *Proc. Natl. Acad. Sci.* **106,** 1954–1959 (2009).
47. Wibberg, D. *et al.* Establishment and interpretation of the genome sequence of the phytopathogenic fungus Rhizoctonia solani AG1-IB isolate 7/3/14. *J. Biotechnol.* **167,** 142–155 (2013).
48. Min, B. *et al.* Genome sequence of a white rot fungus Schizopora paradoxa KUC8140 for wood decay and mycoremediation. *J. Biotechnol.* **211,** 42–43 (2015).
49. Eastwood, D. C. *et al.* The Plant Cell Wall-Decomposing Machinery Underlies the Functional Diversity of Forest Fungi. *Science (80-.).* **333,** 762–765 (2011).
50. Bao, D. *et al.* Sequencing and Comparative Analysis of the Straw Mushroom (Volvariella volvacea) Genome. *PLoS One* **8,** (2013).
51. Smith, S. Y., Currah, R. S. & Stockey, R. A. Cretaceous and Eocene poroid hymenophores from Vancouver Island, British Columbia. *Mycologia* **96,** 180–186 (2004).
52. Fleischmann, A., Krings, M., Mayr, H. & Agerer, R. Structurally preserved polypores from the Neogene of North Africa: Ganodermites libycus gen. et sp. nov. (Polyporales, Ganodermataceae). *Rev. Palaeobot. Palynol.* **145,** 159–172 (2007).
53. Hibbett, D. S., Grimaldi, D. & Donoghue, M. J. Fossil mushrooms from Miocene and Cretaceous ambers and the evolution of homobasidiomycetes. *Am. J. Bot.* **84,** 981–991 (1997).
54. Poinar, G. O. & Buckley, R. Evidence of mycoparasitism and hypermycoparasitism in Early Cretaceous amber. *Mycol. Res.* **111,** 503–506 (2007).
55. Poinar, G. Bird's nest fungi (Nidulariales: Nidulariaceae) in Baltic and Dominican amber. *Fungal Biol.* **118,** 325–329 (2014).
56. Lepage, B. A., Currah, R. S., Stockey, R. A. & Rothwell, G. W. Fossil ectomycorrhizae from the middle Eocene. *Am. J. Bot.* **84,** 410–412 (1997).
57. Duringer, P. *et al.* The first fossil fungus gardens of Isoptera: Oldest evidence of symbiotic termite fungiculture (Miocene, Chad basin). *Naturwissenschaften* **93,** 610–615 (2006).

58. Knobloch, E. & Kotlaba, F. Trametites eocenicus, a new fossil polypore from the Bohemian Eocene. *Czech Mycol.* **47,** 207–214 (1994).